Fumaric acid production with *Rhizopus oryzae*: quantifying time-dependent variations in catabolic flux

Andre Naude

29086737

CVD 800

Fumaric acid fermentation with *Rhizopus oryzae*: quantifying time-dependent variations in catabolic flux

by

Andre Naude

Dissertation presented in partial fulfilment of the requirements for the degree of

Master of Engineering in Chemical Engineering

at the University of Pretoria

Faculty of Engineering, the Built Environment and Information Technology

Department of Chemical Engineering

University of Pretoria

Supervisor: Prof. W. Nicol

May 2015

Synopsis

A technique for analysing batch fumaric acid fermentations is presented. Off-gas measurements were included in the analysis, which assisted in improving the accuracy by means of data reconciliation due to these extra measurements resulting in an overdetermined mass-balance. Instantaneous rate estimations were obtained through smooth polynomial fits on the consolidated dataset. The primary objective was to use this technique to analyse the metabolic flux distribution as the fermentation progressed. This led to the identification of various metabolic phases that could be exploited for favourable results in future process designs. The secondary objective was to investigate the influence of pH and dissolved oxygen (DO) concentration on the metabolic flux distribution using the described technique, with the focus shifted to differences in instantaneous rate and yield characteristics, rather than accumulative differences.

Three distinct metabolic phases were present during this study. Phase A relates to the adjustment period when changing mediums and is characterised by zero fumaric acid production. Phase B started with the commencement of fumaric acid production; the three major metabolic pathways (fumaric acid, ethanol and respiration) were all active during this phase. Most of the fumaric acid was produced during this stage while ethanol production steadily declined. Phase C started when ethanol production reached zero and therefore only the fumaric acid and respiration pathways were active during this phase.

Unlike with the ethanol pathway, the activity of the respiration pathway did not decline as the fermentation progressed. The diminishing ethanol production was interpreted as inactivation of the anaerobic part of the biomass while the aerobic part remained unaffected. The respiration capacity (0.8 mmol O_2/g biomass.h) was identical for all the DO 60% and 80% fermentations, which suggests that respiration was limited by factors other than the DO. The full respiration capacity was not achieved with limited oxygenation (DO 20%).

Instantaneous fumaric acid yields (0.8 g/g for DO 80%) were high during Phase C, but the high ethanol production during Phase B wasted a major fraction of the glucose which led to low overall fumaric acid yields (0.52 g/g for DO 80%). Zero ethanol production and constant

respiration imply that the fumaric acid yield depends solely on the fumaric acid production rate during Phase C. It was found that this rate was inhibited by the fumarate concentration itself, resulting in lower rates (and yields) at high fumarate concentrations. High pH and DO levels countered this inhibition effect. Based on the results, it is recommended that fermentations should be operated at a pH of 5 and a DO of 80%, and that most of the fumaric acid should be produced during Phase C. This can be achieved by batch fermentations with higher initial glucose concentrations (> 100 g/L), by fed-batch fermentations with late glucose addition or by continuous fermentations with concentrations and pretreatment conditions similar to those of the start of Phase C.

Keywords: *Rhizopus oryzae*, fumaric acid, metabolic flux analysis, DO, pH, immobilisation

Acknowledgements

1. Prof. Willie Nicol is thanked for his financial support towards this research, in addition to his role as an excellent supervisor.

2. The financial support of the National Research Foundation (NRF) is greatly appreciated. Opinions expressed are those of the author and not necessarily attributed to the NRF.

3. Michael Bradfield, Adolf Krige and Deon Brink are thanked for their general assistance in experimental work and for their research insight.

Contents

List of figures

List of tables

Nomenclature

ATCC	American Type Culture Collection	
ATP	adenosine triphosphate	
CECT	Colección Española de Cultivos Tipo	
DO	dissolved oxygen (concentration)	% saturation
EMP	Embden-Meyerhof-Parnas glycolysis pathway	
FADH	flavin adenine dinucleotide	
HPLC	High performance liquid chromatography	
NADH	nicotinamide adenine dinucleotide	
NRRL	Agricultural Research Service Culture Collection	
OD	outer diameter	mm
P:O	ratio of ATP produced per NADH:FADH consumed during oxidative phosphorylation	
r_{ATP}^{E}	rate of ATP production from the ethanol pathway	mmol ATP/g Biomass.h
r_{ATP}^{R}	rate of ATP production from respiration	mmol ATP/g Biomass.h
r_{ATP}^{T}	total rate of ATP production	mmol ATP/g Biomass.h
r_{G}^{E}	rate of glucose consumption towards ethanol production	g/g Biomass.h
r_{G}^{F}	rate of glucose consumption towards fumaric acid production	g/g Biomass.h
r_{G}^{E}	rate of glucose consumption towards respiration	g/g Biomass.h
r_{G}^{T}	total glucose consumption rate	g/g Biomass.h
RID	refractive index detector	
TCA	tricarboxylic acid cycle	
Y_{GF}^{inst}	instantaneous fumaric acid yield	

Greek

σ	standard deviation

1 Introduction

It is common knowledge that most carbon-based products (fuel, polymers, adhesives, solvents, pharmaceuticals, etc.) are produced though various chains of chemical processes that use petroleum-based raw materials. These processes are the result of decades' worth of research and development in the petrochemical industry and are integral to the modern quality of life. However, detrimental environmental effects from the petrochemical industry and the depletion of its raw materials threaten the eventual viability of these processes. In order to alleviate these issues, attention has shifted from the petroleum industry as the sole carbon and energy source towards more sustainable and environmentally beneficial industries, such as renewable biomass, solar power, etc.

One of these up-and-coming industries incorporates the use of a bio-based refinery which produces fuels and carbon products, akin to those of a petroleum-based refinery, that use renewable raw materials and moderate process conditions (Sauer et al., 2008). One of the essential objectives of this bio-refinery is to produce bio-based equivalents of the current C2-C4 platform chemicals which are extensively used in the chemical and polymer industries (Jang et al., 2012).

Maleic anhydride is one of the common C2-C4 platform chemicals produced by petrochemical methods. The total market for maleic anhydride in 2013 was 2 100 kilotons/annum and 50% of all maleic anhydride was used in the production of unsaturated polyester resins (Grand View Research, 2014). Fumaric acid has been proposed as the bio-based substitute for maleic anhydride (Xu et al., 2012). Unsaturated polyester resins produced from fumaric acid are harder and more environmentally friendly than those from maleic anhydride. The prospective bulk alternative use for fumaric acid is as cattle feed acidifier (McGinn et al., 2004) with an expected market size of up to US$2600 million by 2018. Fumaric acid has long been considered to be one of the 12 most important bio-based chemical building blocks by the Department of Energy of the United States of America (Werpy & Petersen, 2004).

Research output regarding the bio-based production of fumaric acid is low when compared with that relating to other organic acids, such as citric acid and succinic acid, and for this

reason yields and productivities are low when compared with these acids (Xu et al., 2012). Downstream processing of fumaric acid produced by *Rhizopus oryzae* has recently been found to be more practical due to a significantly lower solubility when compared with these acids and has boosted ongoing research interest (Roa Engel et al., 2008).

Fumaric acid production by *Rhizopus oryzae* involves the use of three main metabolic pathways: (1) the reductive TCA branch (responsible for fumaric acid accumulation); (2) the ethanol pathway (energy generation); and respiration (high-efficiency energy generation). To achieve economically sustainable fumaric acid production, care has to be taken to ensure that all the energy is generated through respiration rather than the ethanol pathway. This objective can be accomplished through proper flux analysis, the results of which can be applied to direct research towards attaining improved yields (and productivities). Current open literature on fumaric acid production is restricted in this regard, with only batch metabolite profiles being predominately reported.

The objective of this study is to develop the methods and tools required for effective flux analysis of *Rhizopus oryzae* fermentations. This entails integrating and consolidating off-gas measurements with metabolite concentrations in the fermentation broth via a mass-balanced metabolic flux model. This will enable quantification of the carbon distribution as a function of fermenter conditions. The flux characteristics will be pivotal when developing new fermenter designs in which operating conditions and broth concentrations will be optimised for high yield and production of fumaric acid.

The analysis method was developed by employing batch fermentations on immobilised *Rhizopus oryzae* on a polypropylene support. pH and dissolved oxygen (DO) concentration levels were varied to investigate the effect of these external conditions on the flux distribution. Fermentations were performed in a novel, external-recycle reactor. Glucose was used as the carbon source and urea as the nitrogen source. Fermentations were carried out in two stages: a growth stage and a production stage. The metabolic flux analysis was done on the production stage since most of the fumaric acid was produced during this stage. The initial glucose concentration for the production stage was 100 g/L and the fermentation was performed at 35 °C.

2 Theory

2.1 Fumaric acid

Fumaric acid ($C_4H_4O_4$), also known as (E)-2-butenedioic acid or *trans*-1, 2-ethylenedicarboxylic acid, is a four-carbon dicarboxylic acid and is shown in Figure 2-1. The name is derived from the plant from which it was first isolated, *Fumaria officinalis* (Roa Engel et al., 2008). Fumaric acid has a low aqueous solubility (7 g/kg at 25 °C) and low pK_a values (3.03 and 4.44) (Lohbeck et al., 1990), which leads to easier product recovery when compared with other dicarboxylic acids such as succinic acid and maleic acid.

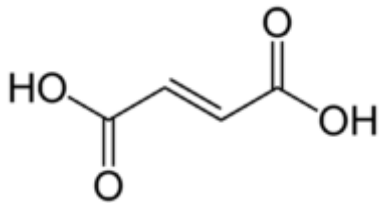

Figure 2-1: Fumaric acid molecule

Fermentation was the main source of fumaric acid in the 1940s but was later discontinued in the 1970s when it was replaced by more competitive petroleum-based processes (Kenealy et al., 1986). In the current commercial process, fumaric acid is produced by catalytic isomerisation of maleic acid. Maleic acid is produced from maleic anhydride, which in turn is produced by catalytic oxidation of butane (Roa Engel et al., 2008).

According to market research, roughly 5% of the total maleic anhydride production is used to produce fumaric acid (Roa Engel et al., 2008). The total maleic anhydride market for 2013 was 2 100 kilotons/annum, which amounts to a fumaric acid market of approximately 105 kilotons/annum. The price of fumaric acid was reported to be US$1.6–1.8 per kg; this is 10% higher than that of maleic anhydride (Mondala, 2015).

Food and beverages accounted for 32% of the global fumaric acid consumption in 2013 (IHS, 2014). It is used as an acidity regulator denoted by the E number E297 (Riscaldati & Moresi, 2002) and is 1.5 times more acidic than citric acid (Xu et al., 2012). Fumaric acid is also an

important intermediate for L-malic acid and L-aspartic acid, both of which are food additives with an increasing market share (Xu et al., 2012).

Other uses include the production of rosin paper sizing and alkyd resins, with 2013 market shares of 20% and 12% respectively (IHS, 2014). However, the market share of these two products is expected to decline due to environmental regulations affecting the use of alkyd resins and rosin paper sizing (IHS, 2014).

The double bond and two carboxylic acid groups in fumaric acid (Figure 2-1) confer on it a high amenability for polymerisation and esterification reactions (Xu et al., 2012). Unsaturated polyester resins make up 18.5% of the fumaric acid market share (IHS, 2014) and account for up to 50% of the total global demand for maleic anhydride (Grand View Research, 2014). Fumaric acid could potentially act as a future replacement for maleic anhydride in unsaturated polyester resins since it has the added advantage of being non-toxic and its polymer structure exhibits greater hardness (Roa Engel et al., 2008). The potential market size for this application is expected to be US$3 300 million by 2020 (Grand View Research, 2014). The only reason maleic anhydride is still favoured over fumaric acid is the higher price of fumaric acid, but this difference is expected to diminish with increasing petroleum prices (Roa Engel et al., 2008).

The other large future bulk application of fumaric acid is as cattle feed acidifier. McGinn et al. (2004) showed that methane emissions from cattle could be reduced by up to 70% when compared with other acidifiers (such as lactic and formic acid) when fumaric acid was used as feed acidifier. This could greatly reduce the total global methane emissions as farm animals are responsible for up to 14% of global methane emissions (McGinn et al., 2004). The total global market for feed acidifiers is expected to be worth US$2 616 million by 2018 (Markets and Markets, 2014).

Due to the increasing demand for fumaric acid (particularly in the Chinese food industry (IHS, 2014)) and rising fuel costs, there has been renewed interest in fumaric acid production by fermentation. Chinese companies such as Changmao Biorefinery and Jiangsu Jiecheng Bioengineering have invested substantial amounts of financial and human resources into microbial production of fumaric acid (Xu et al., 2012). Fumaric acid has been identified as

one of the 12 most important platform chemicals to be produced by industrial fermentation (Werpy & Petersen, 2004), since it would be the bio-based replacement for maleic anhydride.

2.2 Microbial production of fumaric acid

2.2.1 Microorganisms

Fumaric acid is an intermediate metabolite in the tricarboxylic acid (TCA) cycle and is produced in small amounts by numerous microorganisms (Roa Engel et al., 2008). Only a few microbial species are able to excrete fumaric acid in significant quantities (Xu et al., 2012). The first fumaric acid-producing strain, *Rhizopus nigricans*, was discovered by Felix Ehrlich in 1911 (Foster & Waksman, 1939). Foster & Waksman (1939) identified high fumaric acid-producing strains after screening 41 strains from eight different genera. The fumaric acid-producing genera were identified as *Rhizopus*, *Mucor*, *Cunninghamella* and *Circinella*. The genus *Rhizopus*, within the order Mucorales, has been found to contain the only microorganisms that are suitable for industrial production of fumaric acid. The following *Rhizopus* strains have been identified as candidates for industrial production of fumaric acid: *nigricans*, *arrhizus*, *oryzae* and *formosa* (Foster & Waksman, 1939; Rhodes et al., 1962; Kenealy et al., 1986; Cao et al., 1997; Carta et al., 1999).

Not all strains of *Rhizopus oryzae* produce fumaric acid. Abe et al. (2003) classified *Rhizopus oryzae* into two different types. Type I strains produce fumaric acid with little or no lactic acid. Type II strains produce lactic acid with little or no fumaric acid. Therefore for fumaric acid production only type I strains are used; the most prominent among these strains are *Rhizopus oryzae* (ATCC 20344) and *Rhizopus oryzae* (ATCC 52918). These two strains give the highest productivity and product titre, and have been the most widely researched and discussed in the open literature since 1990 (Roa Engel et al., 2008), with *Rhizopus oryzae* (ATCC 20344) being the most widely used strain.

2.2.2 Metabolic pathways

It was first suggested that fumaric acid synthesis in *Rhizopus* species involved a C-2 plus C-2 condensation reaction (Romano et al., 1967). This predicted a maximum yield of 100% on a

molecular basis (64.4% on a mass basis) with glucose as substrate, but it was not in agreement with experimental yields above 100% on a molecular basis (Rhodes et al., 1962). Romano et al. (1967) hypothesised that the reductive branch of the TCA cycle was the main contributor to fumaric acid accumulation. A C-3 plus C-1 mechanism for the fixation of CO_2 was proposed and was later confirmed by ^{13}C nuclear magnetic resonance and enzyme activity studies (Kenealy et al., 1986). The reductive TCA branch responsible for fumaric acid accumulation is located exclusively in the cytosol (Osmani & Scrutton, 1985). The metabolic pathway for fumaric acid synthesis is illustrated in Figure 2-2.

With the reductive TCA pathway, the theoretical yield for fumaric acid is 200% on a molecular basis (128.8% on a mass basis) and is shown by Equation 2-1. The pathway in Equation 2-1 requires CO_2 to be added during fermentation since two moles of CO_2 are fixated per mole of glucose consumed. This pathway is redox and energy neutral, implying zero generation or consumption of NADH (nicotinamide adenine dinucleotide) and ATP (adenosine triphosphate) when the overall pathway is considered; therefore this pathway represents only the theoretical maximum since energy is required for cell maintenance and acid transport (Xu et al., 2012). The maximum fumaric acid yield when no CO_2 is added is 150% on a molecular basis (100% on a mass basis) and the reaction is shown by Equation 2-2. This is achieved by using a combination of the oxidative and reductive TCA pathways (Figure 2-2).

$$C_6H_{12}O_6 + 2\,CO_2 \rightarrow 2\,C_4H_4O_4 + 2\,H_2O \qquad 2\text{-}1$$

$$C_6H_{12}O_6 + 1.5\,O_2 \rightarrow 1.5\,C_4H_4O_4 + 3\,H_2O \qquad 2\text{-}2$$

The energy required for cell maintenance and acid transport is generated in the ethanol and oxidative TCA cycle pathways (Gangl et al., 1991). The ethanol pathway is located in the cytosol of the cell, whereas the oxidative TCA pathway is located in the mitochondrion of the cell (Osmani & Scrutton, 1985). This is illustrated in Figure 2-2. The oxidative TCA pathway is active only under aerobic conditions; oxidative phosphorylation converts all the excess redox (NADH and $FADH_2$ – flavin adenine dinucleotide) generated by the oxidative TCA pathway to energy (ATP) (Gangl et al., 1991). This combination of the oxidative TCA pathway and oxidative phosphorylation will henceforth be referred to as respiration. The reactions for the ethanol and respiration pathways are shown in Equations 2-3 and 2-4

respectively. From these reactions it is evident that respiration is much more energy efficient, generating up to 19 times more ATP per mole of glucose consumed than the ethanol pathway. Equation 2-4 represents the theoretical maximum (P:O ratio of 3), but in practice Equation 2-5 (P:O ratio of 1.25) gives a better indication of the actual respiration performance (Villadsen et al., 2011: 35). Therefore, in practice, respiration generates 9.5 more ATP (energy) per mole of glucose consumed than the ethanol pathway. The difference in ATP generation between the theoretical maximum and the actual amount is due to proton leakage across the mitochondrial membrane and slippage of the ATP synthase proton pump (Villadsen et al., 2011: 142).

$$C_6H_{12}O_6 \rightarrow 2\,C_2H_6O + 2\,CO_2 + 2\,ATP \qquad 2\text{-}3$$

$$C_6H_{12}O_6 + 6\,O_2 \rightarrow 6\,CO_2 + 6\,H_2O + 38\,ATP \qquad 2\text{-}4$$

$$C_6H_{12}O_6 + 6\,O_2 \rightarrow 6\,CO_2 + 6\,H_2O + 19\,ATP \qquad 2\text{-}5$$

Song et al. (2011) did biochemical assays on the mitochondrial and cytosolic fumarase. It was found that the cytosolic fumarase had a higher affinity for the conversion of malic acid into fumaric acid than the mitochondrial fumarase. This suggests that there might be two genes that encode two different fumarases in *Rhizopus oryzae*, one in the cytosol (reductive TCA branch) and another in the mitochondrion (oxidative TCA cycle). Ding et al. (2011) showed that cytosolic fumarase is inhibited by the nitrogen source (urea and yeast extract) and therefore nitrogen limitation is important for fumaric acid accumulation.

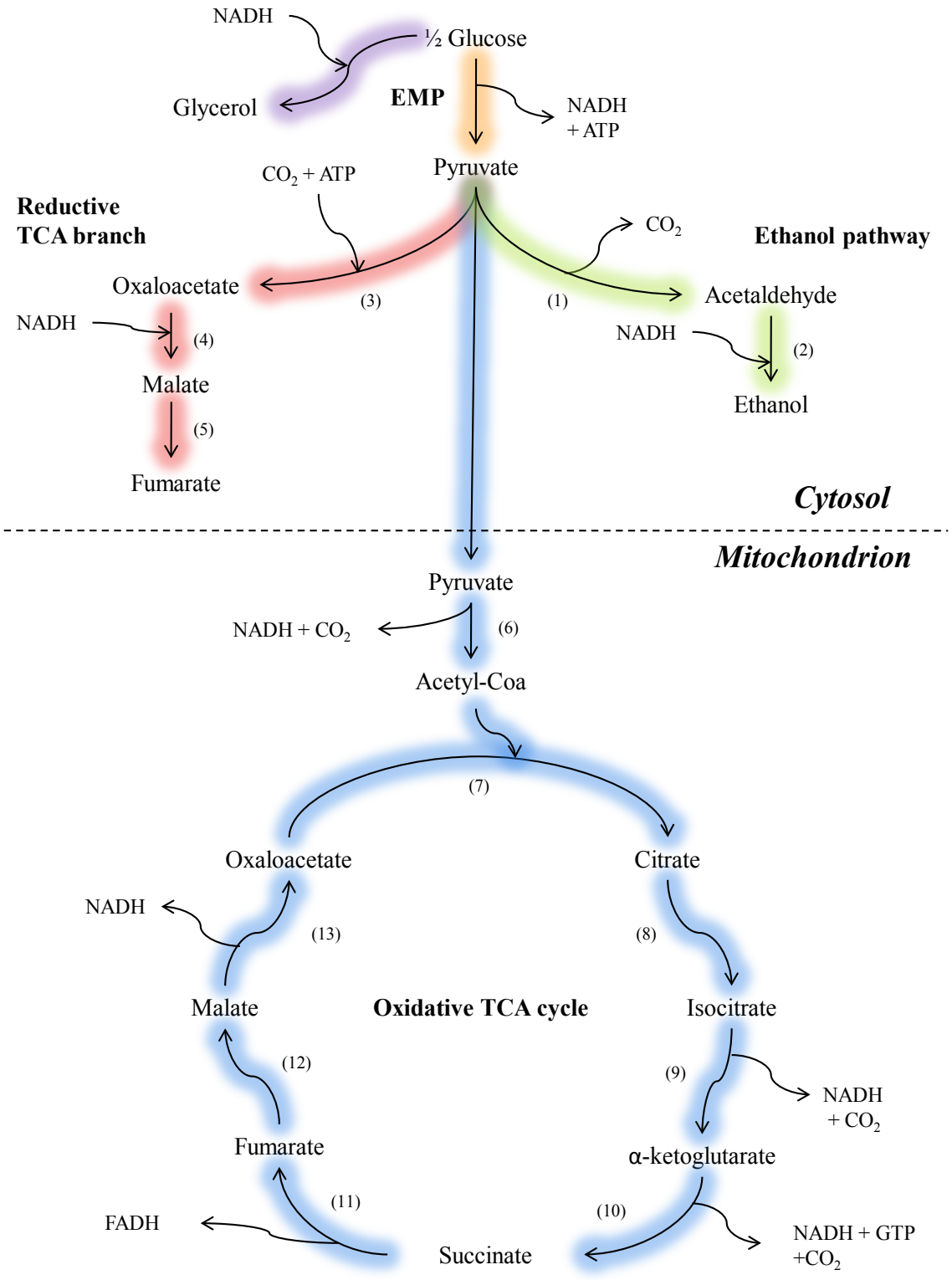

Figure 2-2: Metabolic pathways for *Rhizopus oryzae* (ATCC 20344)
Enzymes are indicated by bracketed numbers: 1. Pyruvate decarboxylase, 2. Alcohol dehydrogenase, 3. Pyruvate carboxylase, 4. Malate dehydrogenase, 5. Fumarase, 6. Pyruvate dehydrogenase complex, 7. Citrate synthase, 8. Aconitase, 9. Isocitrate dehydrogenase, 10. α-ketoglutarate dehydrogenase and succinyl-CoA synthase, 11. Succinic dehydrogenase, 12. Fumarase, 13. Malate dehydrogenase.

2.3 Aspects of fumaric acid fermentation

2.3.1 General fermentation strategy

Almost all fumaric acid fermentations with *Rhizopus oryzae* are done in a two-stage method (Roa Engel et al., 2011). Typical values used by Roa Engel et al. (2011), Du et al. (1997), Cao et al. (1997) and Zhou et al. (2002) are given in brackets. The first stage, referred to as the growth stage, has a limited amount of carbon (5–20 g/L glucose) since high glucose concentrations (> 20 g/L) prevent biomass growth due to high osmotic pressure (Xu et al., 2012). This stage has a high nitrogen content (2 g/L urea); this promotes biomass growth and is therefore responsible for most of the biomass produced during the two-stage operation. The pH in this stage (3–5) is usually lower than that of the second stage (5–6) in order to achieve the required morphology (Roa Engel et al., 2011).

The objective of the second stage is to maximise fumaric acid production. The second stage, referred to as the production stage, has a high amount of carbon (100 g/L of glucose) and very low or no nitrogen content. This promotes fumaric acid production (Song et al., 2011) since no carbon is directed towards biomass growth and this prevents the inhibition of the cytosolic fumarase enzyme from the nitrogen source (Ding et al., 2011). It is also possible to prevent biomass growth by phosphate limitation (Riscaldati et al., 2000). pH control during this stage is very important (Roa Engel et al., 2011) since most of the fumaric acid is produced in this stage.

2.3.2 Morphology

Morphology control is a major challenge in achieving high yield and productivity. In submerged fermentations the three main morphological forms are clumps, filaments and pellets. These forms are shown in Figure 2-3. Fungal morphology is difficult to control since it is affected by most fermentation variables such as pH, shear, heavy metal content, nitrogen content, temperature, preparation of inoculums and osmotic pressure (Roa Engel et al., 2011). Morphology control of *Rhizopus oryzae* is mostly empirical and data on the subject are limited (Xu et al., 2012). A proper mathematical model for morphological control, such as the

one developed for *Aspergillus niger* (Grimm et al., 2005), is required for proper scale-up for processes using *Rhizopus oryzae* (Xu et al., 2012).

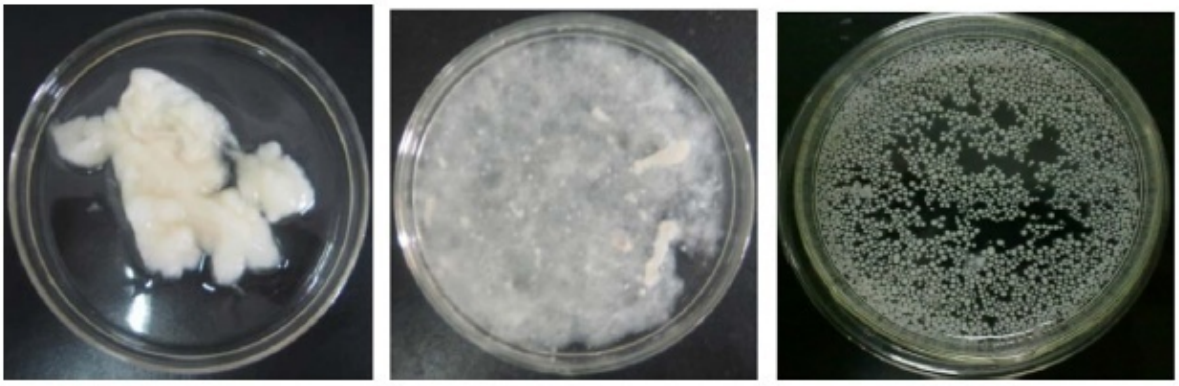

Figure 2-3: Different morphologies in submerged cultures
(Source: Xu et al., 2012)

The morphology of *Rhizopus oryzae* influences the flux distribution towards the main metabolic pathways (ethanol pathway, fumaric acid production and respiration), the nutrient consumption rate and the oxygen uptake rate (Xu et al., 2012). Clump morphology causes internal oxygen limitation in cells, which results in low production of biomass (growth stage) and fumaric acid (production stage) (Zhou et al., 2000) and is therefore rarely used in fermentations (Roa Engel et al., 2011).

Filamentous growth with highly branched mycelia is favourable for the production of enzymes such as amylase, pectinase, xylanase and cellulase (Ghosh & Ray, 2011), and is the preferred morphology when using *Rhizopus oryzae* with starch as carbon substrate (Deng et al., 2012). The disadvantage of filaments is increased viscosity of the fermentation medium. Addition of carboxymethyl cellulose to the growth medium results in higher, more dispersed mycelia with improved oxygen transfer, which increases fumaric acid production by up to 300% (Morrin & Ward, 1990).

Pellets have the highest fumaric acid yield due to their improved oxygen-transfer capability. Small pellets (1 < mm) have shown the best performance (Zhou et al., 2000). The other advantage of pellets is their lower viscosity compared with filamentous morphology and that the pellets can be reused (Liao et al., 2007). Pellet formation can be divided into two categories: aggregation and non-aggregation. The aggregation form is due to multiple spores

that combine to form pellets, while the non-aggregation form is the result of pellet formation from a single spore (Xu et al., 2012).

2.3.3 pH

Several studies have been done to determine the optimum pH for both the biomass growth stage and the fermentation stage. Effective pH control is required during both of these stages since the pH influences the morphology of the biomass, the productivity and the metabolic flux distribution (Roa Engel et al., 2011). The pH and choice of neutralising agent also impact the recovery costs of fumaric acid, which is an important factor in industrial fumaric acid production (Roa Engel et al., 2011).

In the cultivation stage, the optimum pH for pellet morphology was found to be between 3 and 3.3 (Zhou et al., 2000; Fu et al., 2009; Roa Engel et al., 2011). The pellets were hairy and had diameters of less than 1 mm, which improved O_2 transfer and resulted in the highest fumaric acid concentration and yield in their respective studies. The pellets produced by Roa Engel et al. (2011) and Zhou et al. (2000) are shown in Figure 2-4. Zhou et al. (2000) and Fu et al. (2009) found that spores did not germinate at a pH lower than 2.5. The optimum pH for filament morphology is 4 (Zhou et al., 2000; Fu et al., 2009). At a pH above 4.5, clumps start to form, resulting in very low fumaric acid production (Zhou et al., 2000; Fu et al., 2009; Roa Engel et al., 2011).

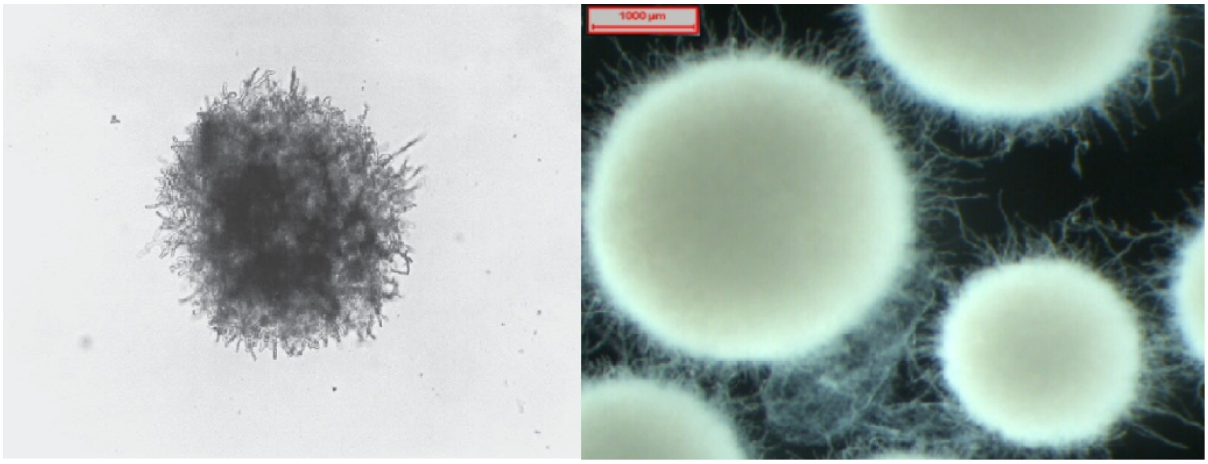

Figure 2-4: Pellets at optimum pH
Zhou et al. (2000) left and Roa Engel et al. (2011) on the right

Roa Engel et al. (2011) found that a pH of 5 during the production stage resulted in the highest fumaric acid yield and titre. Their study also showed the importance of proper pH control. With pH controlled at 5, the amount of fumaric acid produced was 30.21 g/L, while without pH control the amount of fumaric acid produced was 2.92 g/L since the fermentation stopped when the pH dropped to below 2.4.

2.3.4 Immobilisation

Free-cell fermentations of *Rhizopus oryzae* often lead to large clumps or pellets which cause difficulties such as impeding of impellers, fouling of agitation blades, blocking of the sampling and feeding ports, and low yields due to oxygen limitation. To address these problems *Rhizopus oryzae* can be immobilised onto an attachment surface (Fu et al., 2009).

Petruccioli et al. (1996) used a polyurethane sponge to immobilise *Rhizopus oryzae* in repeat batch fermentations. The productivity (0.256 g/L.h) and fumaric acid titre (12.3 g/L) were lower than those of conventional submerged fermentations. The main advantages were that it was easy to reuse the immobilised fungi and that the fungi lasted for several batches (8) before productivity started to decline.

Gu et al. (2013) used a wire-and-fibre net to immobilise *Rhizopus oryzae* and compared it with conventional free-cell fermentations. The immobilised and free-cell fermentations had similar fumaric acid titres, namely 31.23 g/L and 32.03 g/L respectively, while the immobilised cells had much higher productivity (1.3 g/L.h) than the free cells (0.217 g/L.h). The claimed increase in productivity was due to increased biomass density as a result of immobilising the fungi on the net.

Cao et al. (1997) attached *Rhizopus oryzae* to plastic rotating discs. The productivity (3.78 g/L.h) was increased since the cells were exposed to both the gas and liquid phases of the reactor and resulted in the highest productivity of any fumaric acid fermentation without using *in situ* product recovery. The advantage of immobilisation is that the attached fungi are reused in repeat batch fermentations.

2.4 Fumaric acid production studies

All studies on fumaric acid production occurred under batch, semi-batch and repeat batch conditions. No studies of continuous operation have been reported. This is due to the operational difficulties when working with free fungal cells. Repeat batch fermentations are only possible with immobilised cells (Cao et al., 1997). Table 2-1 contains a summary of fumaric acid studies done with wild *Rhizopus oryzae* strains.

The highest yield (0.82 g/g), titre (107 g/L) and productivity (2 g/L.h) for a submerged fermentation were obtained by Ng et al. (1986) using *Rhizopus oryzae* ATCC 52918. Efficient morphology control resulted in small pellets with a good oxygen uptake rate. Biotin, a cofactor of the enzyme pyruvate carboxylase (Figure 2-2), was added to improve the metabolic flux rate towards the reductive TCA branch, which resulted in high fumaric acid productivity and yield. The fermentation was performed at a pH of 6.

Du et al. (1997) used an airlift reactor with high oxygen mass transfer and compared the results with those of a traditional submerged fermentation. The pH was controlled at 5 and $CaCO_3$ was used as neutralising agent and CO_2 source. The oxygen mass transfer coefficient was three times higher for the airlift reactor than for the submerged reactor. The dissolved oxygen (DO) level in the airlift reactor remained at 90%, but the DO level for the submerged fermentation was not reported. The airlift reactor had a higher yield and productivity (0.754 g/g and 0.814 g/L.h) than those of the submerged fermenter (0.60 g/g and 0.66 g/L.h).

Cao et al. (1996, 1997) used a rotating biofilm contactor reactor consisting of rotating plastic discs with a thin film of immobilised fungi grown on them. The discs rotated so that the fungi were exposed to both the gas and liquid phases of the reactor. This reactor, along with the use of *in situ* product recovery of fumaric acid, achieved the highest yield (0.86 g/g) and productivity of any study (4.25 g/L.h). The titre is lower than that of Ng et al. (1986) due to the lower concentration of glucose used. These results were obtained without using a CO_2 source and the yield is therefore within 86% of the theoretical maximum (1 g/g) when no CO_2 is added to the system. Since the fungi were immobilised, there was the added advantage that they could be reused in a repeat batch process. The fungi were used for four cycles before being regenerated.

Table 2-1: Fumaric acid studies done on wild strains of *Rhizopus*.
(Adapted from Roa Engel et al., (2008) and (Xu et al., 2012)

Strain	Fermenter	Substrate	Product titre (g/L)	Productivity (g/L.h)	Yield (g/g)	Reference
R. nigricans	Shake flask	Glucose	14	-	0.50	(Foster & Waksman, 1939)
45	Shake flask	Glucose	20	0.25	0.66	(Romano et al., 1967)
R. oryzae[D]	Stirred tank[a]	Glucose	90	1.22	0.70	(Rhodes et al., 1962)
ATCC 52918 or	Stirred tank[a]	Glucose	107	2.00	0.82	(Ng et al., 1986)
NRRL 2582	Stirred tank	Glucose	73	0.50	0.72	(Gangl et al., 1990)
R. oryzae[D]	Shake flask	Glucose	98	1.02	0.81	(Kenealy et al., 1986)
ATCC 12732 or	Fluidised bed	Molasses	18	0.36	0.36	(Petruccioli et al., 1996)
NRRL 1526	Stirred tank	Glucose	38	0.46	0.33	(Riscaldati et al., 2000)
R. oryzae	RBC[B]	Glucose	76	3.78	0.75	(Cao et al., 1997)
ATCC 20344 or	RBC[C]	Glucose	92	4.25	0.85	(Cao et al., 1996)
NRRL 6400	Airlift	Glucose	38	0.81	0.75	(Du et al., 1997)
	Bubble column	Glucose	37	1.03	0.53	(Zhou et al., 2002)
	Stirred tank	Dairy manure	31	0.32	0.31	(Liu et al., 2008)
	Stirred tank	Glucose	56	0.70	0.54	(Fu et al., 2010)
	Stirred tank	Glucose	41	0.37	0.48	(Huang et al., 2010)
	Stirred tank	Glucose	32	0.32	0.45	(Kang et al., 2010)
	Stirred tank	Glucose	30	0.19	0.28	(Roa Engel et al., 2011)

[A] Biotin was added to the fermentation medium

[B]Rotary biofilm reactor

[C]Rotary biofilm reactor with *in situ* product recovery by adsorption

[D]Formerly known as *Rhizopus arrhizus* (Abe et al., 2003)

3 Experimental

3.1 Microorganism and growth

The microorganism used in this study was *Rhizopus oryzae* (ATCC 20344 or NRRL 6400) from the Spanish Collection of Cultures, Colección Española de Cultivos Tipo (CECT), Valencia, Spain. The culture was grown at 35 °C on potato dextrose agar plates (Merck) to produce spores. After 96 hours, the agar plates were washed with sterilised water to obtain a spore solution. The spore solutions were stored at 4 °C; new spore solutions were prepared every 3 months.

Cultures were tested for purity and viability by preparing 200 mL solutions of sterilised tryptone soy broth and inoculating them with the spore solution. A high-performance liquid chromatography (HPLC) analysis was done after 48 hours to determine whether the spore solutions were pure and viable.

3.2 Fermentation media

A two-stage fermentation method was used as in previous fermentation studies (Roa Engel et al., 2011; Cao et al., 1996; Cao et al., 1997; Du et al., 1997; Zhou et al., 2002). The medium components are shown in Table 3-1 and were identical to those of previous studies (Roa Engel et al., 2008; Cao et al., 1996; Cao et al., 1997; Du et al., 1997; Zhou et al., 2002), except for the glucose concentration during the growth stage since using 10 g/l of glucose would lead to excessive biomass blocking. The heavy metal concentrations used in this study and the abovementioned studies were based on an optimisation study done by Zhou et al. (2000).

Distilled water was used and the medium was sterilised in an autoclave at 121 °C for 60 minutes. The glucose and urea were each sterilised separately from the rest of the components. All the components in Table 3-1 were obtained from Merck, South Africa. Instrument-grade air (Afrox, South Africa), a dry mixture of synthetic air (20% O_2 and 80% N_2), was used for sparging air through the reactor.

Table 3-1: Media components used in this study

Fermentation stage	Component	Concentration (g/L)
Growth stage	Glucose	5.000
	Urea	2.000
	KH_2PO_4	0.600
	$MgSO_4.7H_2O$	0.250
	$ZnSO_4.7H_2O$	0.088
Production stage	Glucose	100.000
	KH_2PO_4	0.600
	$MgSO_4.7H_2O$	0.250
	$ZnSO_4.7H_2O$	0.088
	Yeast extract	1.000

3.3 Reactor set-up

The reactor consists of a 50 mm outside diameter (OD) glass cylinder contained between an aluminium base and head. The working volume of the reactor was 220 mL. A polypropylene pipe 34 mm in diameter was used as attachment surface for the fungi. It had a length of 170 mm and fungi were attached on both sides of the cylinder. The reactor base had three ports and the reactor top had five ports. The reactor set-up is shown in Figure 3-1 and Figure 3-2.

Agitation was achieved by using an external recycle line from the head of the reactor to the base of the reactor. The recycle pump (Wason Marlow 323U) switches direction every 30 seconds. This ensures that there is no accumulation of fungi on the low-pressure side of the recycle pump and also improves the mixing in the reactor. The flow rate of the recycle pump was set at 120 mL/min.

All the components of the reactor system (feed bottles, pH probes, reactor vessel, etc.) were connected by 5 mm silicone tubing, and 10 mm polypropylene T-pieces were used where required. Peristaltic pumps (Watson Marlow 120U) were used as inlet, outlet and dosing

pumps. The average dosing flow rate was monitored using Labview. All product bottles and feed bottles, as well as the reactor vessel, were vented to atmosphere and 0.2 µm PTFE filters were used to prevent contamination.

The temperature was controlled at 35 °C by a hotplate (Agimatic-N) connected to a temperature controller (Heidolph EKT 3005) which used a thermocouple (Heidolph Type K) connected in the recycle line. The pH was measured using a CPS 471D ISFET pH probe (Endress & Hauser) housed in an aluminium probe holder connected in the recycle line. The pH probe was connected to a Liquiline CM 442 (Endress & Hauser) transmitter. The pH was controlled by using a relay on the Liquiline CM 442 transmitter to switch the dosing pump on/off. 3M NaOH was dosed in order to control the pH.

The flow of air into the reactor was controlled using a SLA5850 (Brooks) gas controller. The air flow rate into the reactor was controlled at 22 mL/min (10% vvm). The DO level in the reactor was measured using a COS 22D (Endress & Hauser) DO probe housed in an aluminium probe holder connected in the recycle line. The DO probe was connected to a Liquiline CM 442 transmitter. The DO was controlled by a relay on the Liquiline CM 442 transmitter to switch the air recycle pump on/off. The air recycle pump takes the air leaving the top port of the reactor and recycles it back into the sparger. The air recycle pump flow rate was 660 mL/min (3 vvm).

The following variables were recorded on line using a custom Labview application: temperature, pH, DO, average dosing flow rate, air recycle flow rate and air inlet rate. These variables were used to ensure that there were no disturbances during a fermentation that could affect the results.

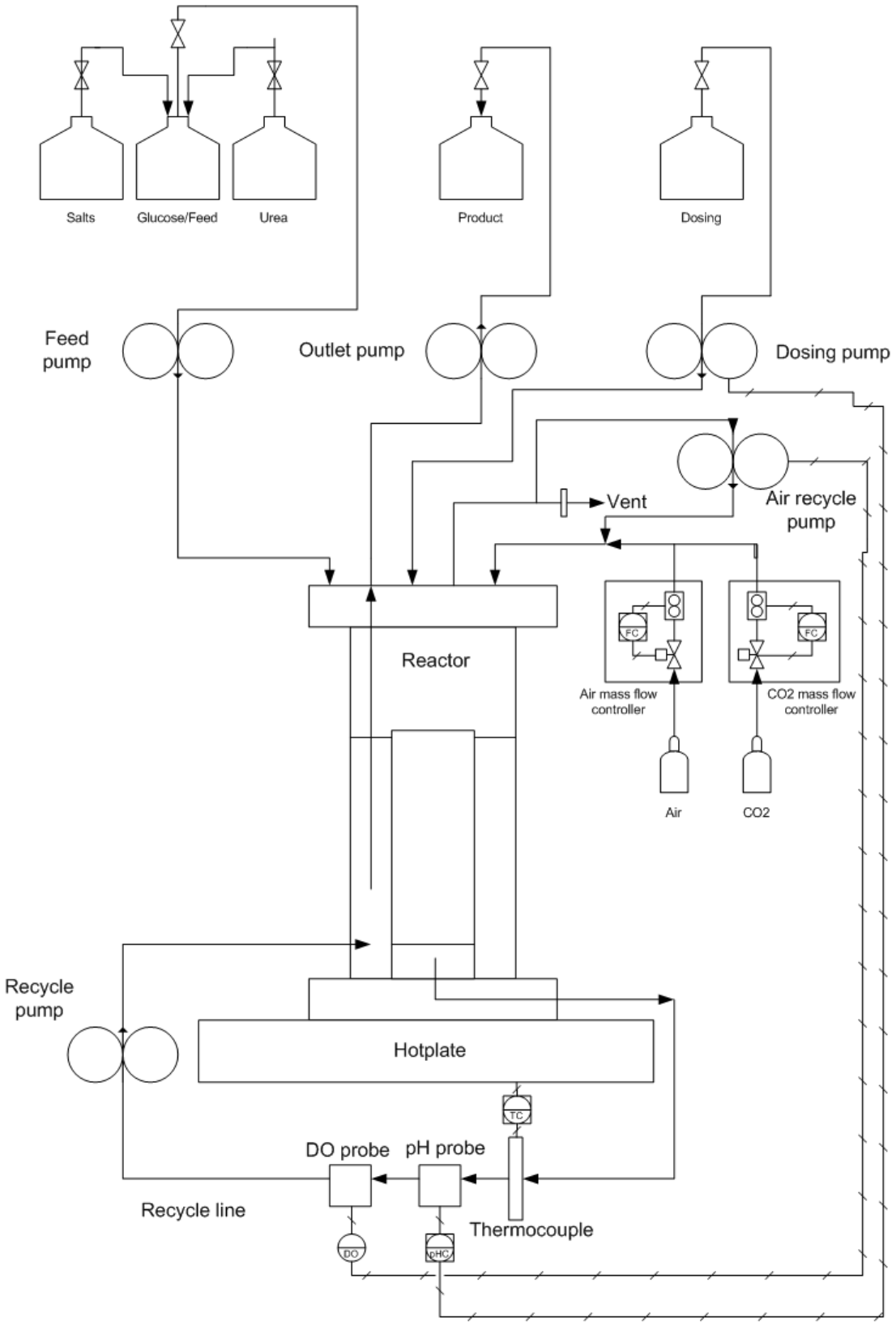

Figure 3-1: Reactor set-up used in the study

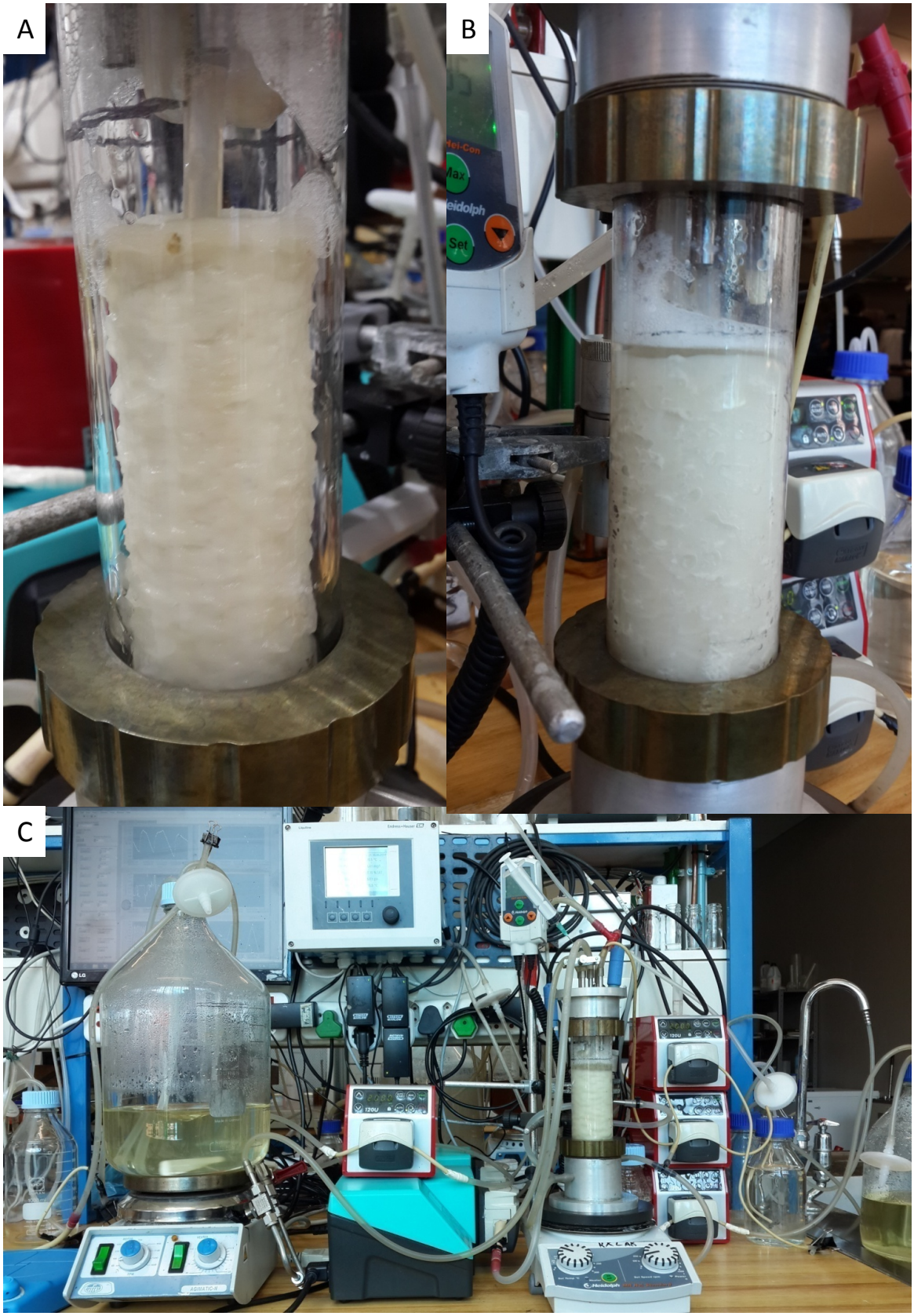

Figure 3-2: Images of the fermenter set-up.
Image A was taken at the end of the growth stage, image B was taken during the fermentation stage and image C shows the reactor set-up

3.4 Analytical methods

3.4.1 HPLC analysis

Glucose, fumaric acid, ethanol, malic acid, glycerol and succinic acid were determined using an Agilent 1260 Infinity HPLC (Agilent Technologies, USA) with an Aminex HPX-87H column (Bio-Rad Laboratories, USA) and a refractive index detector (RID). The mobile phase was 0.3 ml/L H_2SO_4 with a flow rate of 0.6 mL/min at a temperature of 60 ^oC.

3.4.2 Gas analysis

The gas composition (CO_2 and O_2) was measured using a Tandem (Magellan Biotech, UK) gas analyser. The air was dried before it entered the gas analyser in order to remove the effects of water and ethanol vapour from the measurement and the gas compositionwas recorded every second.

3.4.3 Biomass measurement

The final biomass was filtered on preweighed filter paper (Whatman, 47 mm) and washed with distilled water. The biomass was left to dry at 90 ^oC for 24 hours and then weighed to yield the final amount of dry biomass.

3.5 Metabolic flux model

The mathematical metabolic flux model is based on the metabolic pathways shown in Figure 2-2 and was built using the methods proposed by Villadsen et al. (2011: 180). The model simplifies the pathways of Figure 2-2. It is shown in Figure 3-3 and illustrates how the equations for the mathematical model were derived.

The model has ten variables. There are eight measured variables: glucose (V1), glycerol (V10), ethanol (V4), fumaric acid (V5), malic acid (V6), succinic acid (V7), CO_2 (V8) and

O_2 (oxidative phosphorylation) (V9). The two calculated values are the oxidative TCA pathway (V2) and the pyruvate pathway (V3).

The model has four equations, which implies that the system is overspecified by two. This overspecification can be used for data reconciliation to obtain more accurate measured rates (Section 3.6). The two first equations are carbon balances around nodes 1 and 2 in Figure 3-3 and are given by Equation 3-1 and Equation 3-2 respectively.

$$-V_1 + V_{10} + V_2 + V_3 = 0 \qquad 3\text{-}1$$

$$-V_3 + 1.5\,V_4 + 0.75\,V_5 + 0.75\,V_6 + 0.75\,V_7 = 0 \qquad 3\text{-}2$$

The third equation is an NADH balance over the entire system shown in Figure 3-3 and is given by Equation 3-3.

$$-\frac{1}{3}V_{10} + 2\,V_2 + \frac{1}{3}V_3 - \frac{1}{2}V_4 - \frac{1}{4}V_6 - \frac{1}{2}V_7 - 2\,V_9 = 0 \qquad 3\text{-}3$$

The final equation relates the measured CO_2 (V8) to all of the CO_2 released or fixed by the pathways in Figure 3-3 and is given by Equation 3-4.

$$V_8 - V_2 - 0.5\,V_4 + 0.25\,V_5 + 0.25\,V_6 + 0.25\,V_7 = 0 \qquad 3\text{-}4$$

Maintenance is the energy (ATP) consumed by the cell in order to sustain itself and is a very important factor in fermentation analysis as it gives an indication of the efficiency of the cells when investigating different reactor conditions (Villadsen et al., 2011: 173). The ATP generation rate (r_{ATP}) is determined by calculating the excess ATP produced (i.e. ATP that is not consumed by the formation of metabolites) through substrate consumption and is given by Equation 3-5.

$$r_{ATP} = \frac{1}{3}V_2 + \frac{1}{3}V_3 - \frac{1}{4}V_5 - \frac{1}{4}V_6 - \frac{1}{4}V_7 + 2\frac{P}{O}V_9 \qquad 3\text{-}5$$

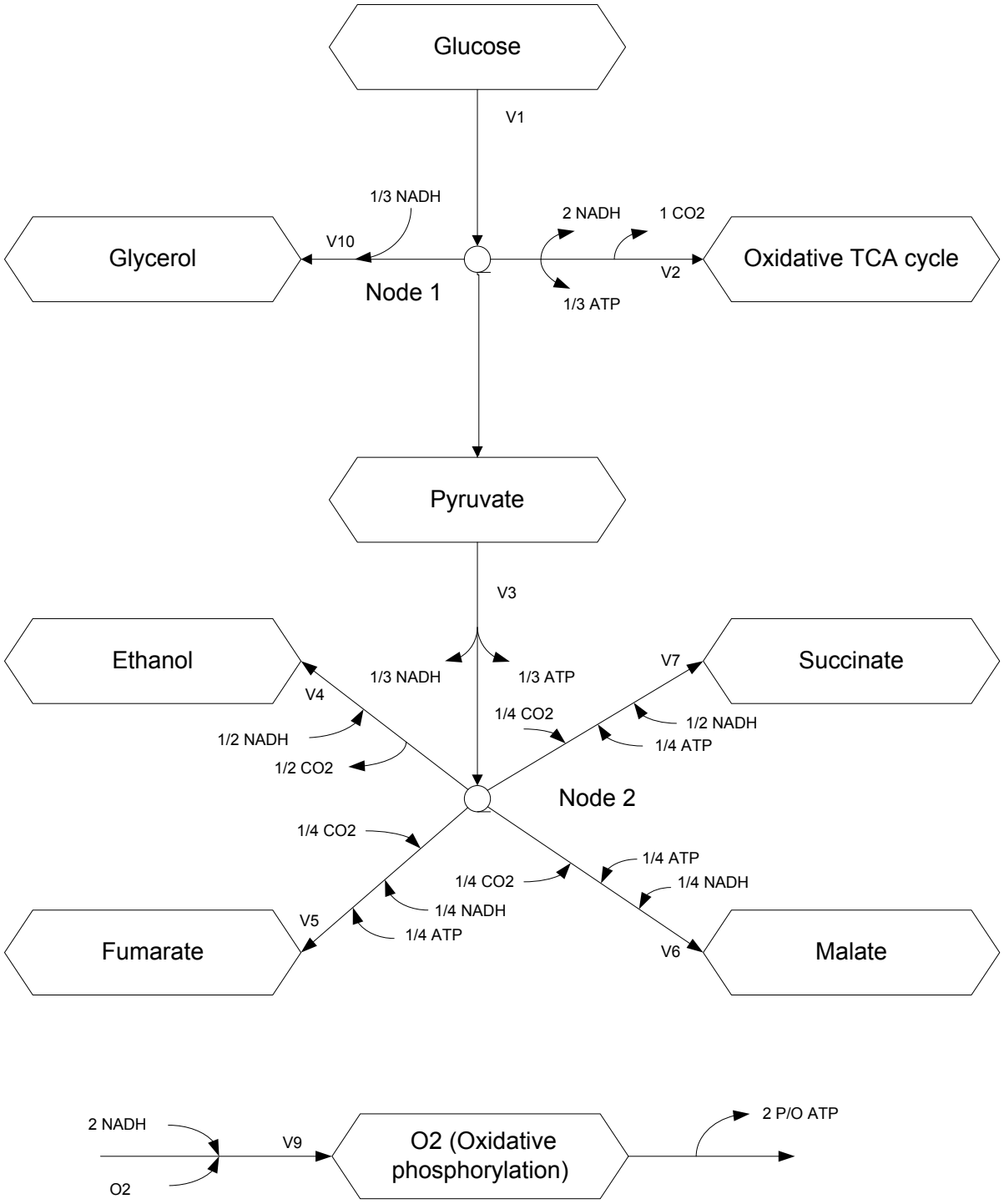

Figure 3-3: Simplified metabolic flux model used to build the mathematical model

3.6 Data reconciliation

Data reconciliation uses extra measurements in order to identify gross (non-random) measurement errors and to give better values for these measurement errors. As stated in Section 3.5, there are two extra measurements in this study and therefore data reconciliation can be applied to improve the accuracy of the whole dataset. The data reconciliation method is based on that described by Villadsen et al. (2011: 100).

3.6.1 Measurement errors

There was a total of eight measured variables (glucose, ethanol, fumaric acid, malic acid, glycerol, succinic acid, CO_2 and O_2) in this study. To perform data reconciliation, an estimation of the size and nature of the errors for each of these measurements has to be provided (Villadsen et al., 2011: 100).

The amount of base added was recorded and its diluting effect on the glucose consumed and the production of each of the metabolites was included with each HPLC sample. The amount of substrate or product lost due to sampling and purging was also included with each HPLC sample. The HPLC sample analyses were repeated four times to lessen the number of random errors. The expected error for all HPLC samples, with the exception of ethanol, was calculated as 0.0007 g (this is the base error made by HPLC if exactly the same sample were to be run numerous times) + 2% of the total number measured (this represents the random errors made when preparing the samples). For ethanol the error was calculated as 0.0007 g + 5% of the total number measured. The increased percentage error for the ethanol measurement is due to the evaporation of ethanol.

The error for the gas analysis was expected to be 10% of the total number measured. This is due to the low CO_2 concentration in the outlet gas which could lead to errors since the gas analyser was designed for the high CO_2 concentrations (5% to 20%) usually found in other aerobic fermentations. The low CO_2 concentration in the outlet is due to CO_2 fixation when fumaric acid is formed.

3.6.2 Reconciliation procedure

The measured flux vector, q_m, consists of the following fluxes (flux numbers from Figure 3-3 are shown in parenthesis):

1. Glucose (V1)
2. Fumaric acid (V5)
3. Ethanol (V4)
4. Malic acid (V6)
5. Glycerol (V10)
6. Succinic acid (V7)
7. CO_2 (V8)
8. O_2 (V9)

The calculated flux vector, q_c, consists of the following fluxes:

1. Oxidative TCA pathway (V2)
2. Pyruvate pathway (V3)

The first step is to create the coefficient matrices for the measured variables, E_m, and the calculated variables, E_c. Each column represents the measured/calculated fluxes and each row represents the following equations:

1. Mass balance at Node 1 (Equation 3-1).
2. Mass balance at Node 2 (Equation 3-2).
3. CO_2 (Equation 3-4)
4. NADH balance (Equation 3-3).

The coefficient matrices for the measured variables and calculated variables are given by Equation 3-6 and Equation 3-7 respectively. In this study the P:O ratio (ATP produced per NADH consumed during oxidative phosphorylation) was 1.25 as suggested by Villadsen et al. (2011: 35). The maximum amount of ATP generated from the oxidative TCA cycle and oxidative phosphorylation using this assumption is shown by Equation 2-5.

$$E_m = \begin{matrix} -1 & 0 & 0 & 0 & 1 & 0 & 0 & 0 \\ 0 & 0.75 & 1.50 & 0.75 & 0 & 0.75 & 0 & 0 \\ 0 & 0.25 & -0.50 & 0.25 & 0 & 0.25 & 1 & 0 \\ 0 & -0.25 & -0.50 & -0.25 & -0.333 & -0.5 & 0 & -2 \end{matrix} \quad 3\text{-}6$$

$$E_c = \begin{matrix} 1 & 1 \\ 0 & -1 \\ -1 & 0 \\ 2 & 0.33 \end{matrix} \quad 3\text{-}7$$

The next step is to calculate the redundancy matrix, R. This is given by Equation 3-8. The rank of R shows the number of independent equations – in this case it was two.

$$R = E_m - E_c({E_c}^T E_c)^{-1} {E_c}^T E_m \quad 3\text{-}8$$

R_r is the reduced redundancy matrix containing only the independent rows of R. F is called the variance co-variance matrix. The expected measurement error of each flux is added into the diagonal of the matrix. Since the measurements are all independent of one another, there are no non-diagonal entries. P is used to calculate the minimisation problem in order to determine the estimated error vector and is shown in Equation 3-9.

$$P = R_r F {R_r}^T \quad 3\text{-}9$$

The estimated error vector, δ, is given by Equation 3-10.

$$\delta = F {R_r}^T P^{-1} R_r q_m \quad 3\text{-}10$$

The consolidated measured flux vector, q_m^{Con}, is given by Equation 3-11.

$${q_m}^{Con} = q_m - \delta \quad 3\text{-}11$$

The consolidated calculated flux vector, q_c^{Con}, is given by Equation 3-12.

$${q_c}^{Con} = -\left({E_c}^T E_C\right)^{-1} \left({E_c}^T E_M\right) {q_m}^{Con} \quad 3\text{-}12$$

3.7 Experimental intent

The metabolic flux analysis based on consolidated measurements was performed on the production stage of the batch fermentation. The fermentations of Roa Engel et al. (2011) and Cao et al. (1997) were used to develop the growth strategy and to determine the baseline operating conditions as shown in Sections 3.1 and 3.2. In addition to quantifying the metabolic flux, the effects of pH and DO were investigated. For pH a baseline of 5 was chosen since studies by Roa Engel et al. (2011) and Cao et al. (1997) suggest that this is the optimum pH for both fumaric acid production rate and fumaric acid yield. For DO a baseline of 60% saturation was chosen since this is the level beyond which a higher concentration of dissolved oxygen (> 60%) does not usually result in increased production rates or yields, although it does mean a more expensive process due to the increased aeration costs (Villadsen et al., 2011: 458). Since the baseline conditions were used for all growth stages, the analysis was done only on the production stage.

The pH range used in the study was 4 and 5. This range was chosen since Roa Engel et al. (2011) suggest that using a pH lower than the optimum pH of 5 could lead to a more economical process. The DO range used in this study was 20%, 60% and 80%. The 20% level was chosen due to a patent by Du Pont (Ling & Ng, 1989) suggesting that a DO level of less than 30% is the most economical for fumaric acid production. The 80% level was used to investigate whether there were any benefits to operating at the maximum aeration rate of the current set-up.

4 Results

4.1 Mass balance analysis and data reconciliation

4.1.1 Mass balance analysis

The following components were measured during the production stage: glucose, fumaric acid, ethanol, malic acid, glycerol, succinic acid, CO_2 and O_2. Biomass could only be determined at the end of the production stage. Since all of the expected carbon products/substrates were measured, a carbon balance was used to determine the accuracy of the data. The carbon balance closures for all the batches are given in Table 4-1. These carbon balances were performed without taking biomass into account since there should be no growth during the production stage.

Table 4-1 Percentage closure of carbon balances for each batch

Batch No.	Details	Carbon balance closure
1 (Baseline)	pH 5, DO 60%	92%
2	pH 4, DO 60%	90%
3	pH 5 , DO 80%	92%
4	pH 5, DO 20%	88%
5 (Baseline repeat)	pH 5, DO 60%	92%

The average closure for all the batches was 90%, with a standard deviation (σ) of 2%. The 90% closure indicates that less substrate was actually consumed than was accounted for and/or more metabolites were produced than accounted for. A 90% closure could also indicate a missing metabolite but this is considered unlikely in this study since all the reported primary metabolites produced by *Rhizopus oryzae* (Roa Engel et al., 2011) were measured.

With the current set-up there were three complications affecting the accuracy of the measurements:

1. The amount of base added to control the pH was higher than what was accounted for. This resulted in a higher count of consumed substrate and a lower count of metabolites produced.
2. The CO_2 measurement had a minor error due to the low CO_2 concentration in the outlet gas which could lead to erroneous measurements since the gas analyser was designed for high CO_2 concentrations (5% – 20%), usually found in other aerobic fermentations. The low CO_2 concentration in the outlet is due to CO_2 fixation when fumaric acid is formed (Figure 2-2).
3. The evaporation of ethanol could lead to a lower measurement of ethanol than what was actually produced. Roa Engel et al. (2011) found that with an ethanol concentration of 5 g/L, an evaporation rate of 0.09 g/L.h (dependent on the sparging method) was measured and led to a lowered ethanol count.

4.1.2 Data reconciliation

Since all the metabolites found in the metabolic flux model in Section 3.5 were measured with acceptable carbon balance closure, the same metabolic flux model was used for data reconciliation and analysis. Data reconciliation, as discussed in Section 3.6, was used to obtain a better estimate of the measured rates since two more variables were measured than what was required to solve the metabolic flux model (Villadsen et al., 2011: 100).

Figure 4-1 shows the differences in fermentation profiles due to data reconciliation for batch 1. The reconciled data in Figure 4-1 substantiate the three complications affecting the accuracy of the measurements. The reconciled profiles indicate that glucose consumption was lower than that measured, the amount of ethanol produced was higher than that measured and the amount of CO_2 produced was higher than the measured amount. This trend was observed for all batches. It is interesting to note that the ethanol measurement appears to indicate gross errors only when the ethanol concentration exceeds 5 g/L in the broth. This suggests that some evaporation takes place at high ethanol concentrations. The reconciled data also showed that O_2 measurement was slightly overpredicted by the gas analyser. The production of all the other metabolites – fumaric acid, malic acid, glycerol and succinic acid –was also slightly higher than the measured values.

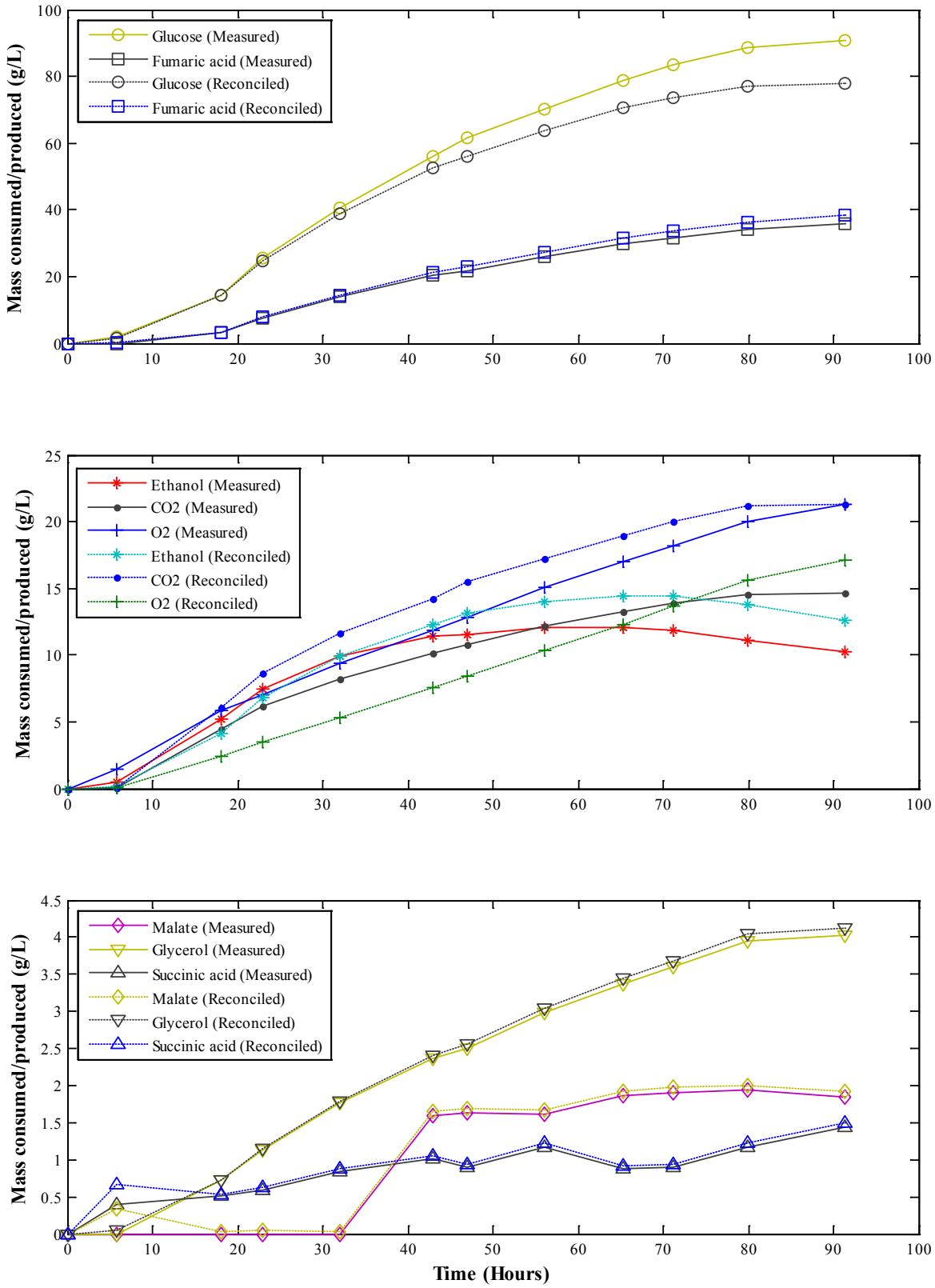

Figure 4-1: Profiles before and after data reconciliation for batch 1

4.2 Repeatability

The next step in the data analysis is to quantify the variance between batches with the same operating conditions. This shows whether a change in the results is due to random variations or due to the change in conditions between experiments. Batch 1 and its repeat experiment, batch 5, are shown in Figure 4-2.

From Figure 4-2 it can be seen that the variations in the glucose, fumaric acid, ethanol, malate, glycerol and succinic acid profiles between the two batches at 50 hours were within 10%. For the gas measurements, O_2 and CO_2, the variations were within 20%. These variations are also attributed to the fact that batch 5 had a longer stationary phase than batch 1. The stationary phase was 5 hours longer for batch 5. Figure 4-3 shows the same profiles as in Figure 4-2, but with the profiles of batch 5 shifted 5 hours to the left. This removes the effect of different stationary phase lengths from the total variance of the data.

From Figure 4-3 it can be seen that the differences in glucose, fumaric acid, ethanol, malate, glycerol and succinic acid between the two profiles at 50 hours were within 5%. The differences in the gas measurements, O_2 and CO_2, also decreased to 15%. When analysing the data it is important to distinguish between the variance from the difference in stationary phases, which was found to vary by up to 5 hours between all the batches, and between the variance from the measurements when comparing results. The significant variance in the gas analysis is a result of the low concentration of CO_2 leaving the reactor and the small change between the inlet and outlet O_2 concentrations.

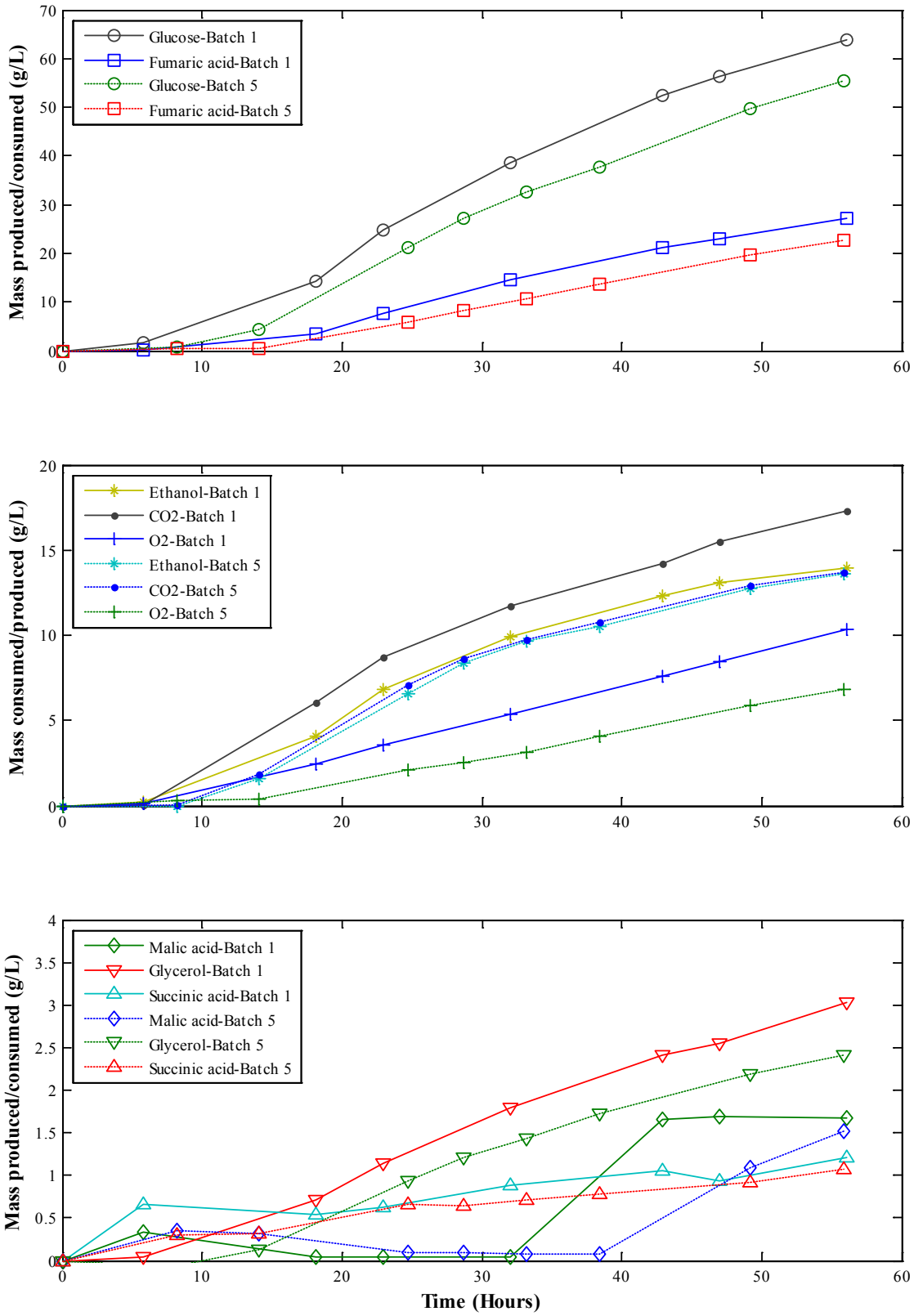

Figure 4-2: Comparison between batch 1 and batch 5
These two batches had the same operating conditions and the graph displays the variance between the two batches; the profiles show the reconciled data.

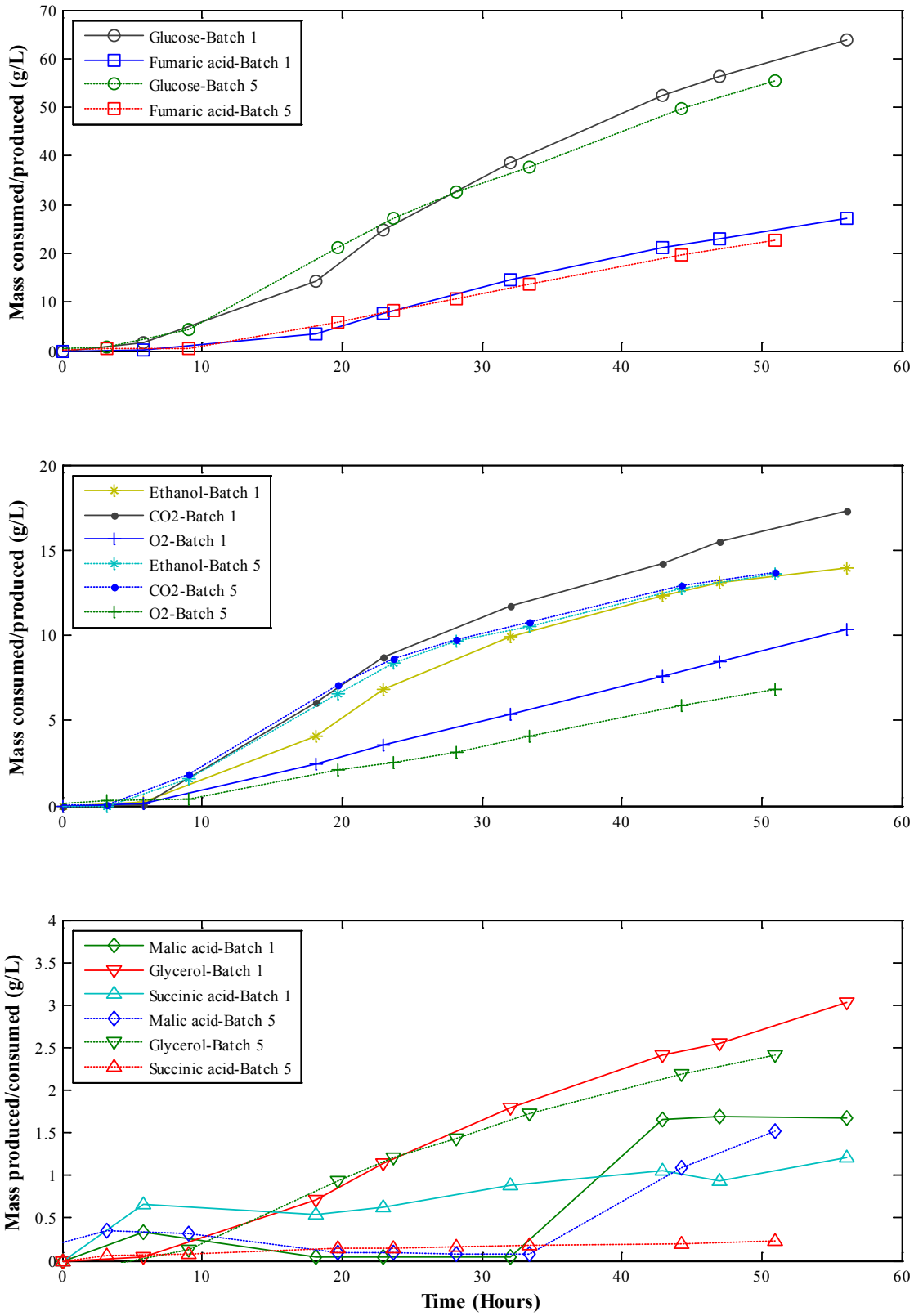

Figure 4-3: Comparison between batch 1 and batch 5
The profiles for batch 5 were shifted 5 hours to the left. This removes the variance due to the different lag times from the total variance between the two batches; the profiles show the reconciled data.

4.3 Measured results

4.3.1 pH results

The profiles for the pH investigation are shown in Figure 4-4. The pH investigation compares batch Nos 1 and 2. Only the main product profiles (fumaric acid, ethanol, O_2 and CO_2) are shown in Figure 4-4 as these profiles represent more than 90% of all the glucose consumed. The minor product profiles (malic acid, succinic acid and glycerol) are given in Appendix A. All the profiles showed good repeatability in terms of their stationary phases and therefore no adjustment was made to the time axis as in Figure 4-3. A summary of the results for the pH investigation is given in Table 4-2. These results show good repeatability with regard to the amount of biomass; therefore any differences in rates in Figure 4-4 can be attributed directly to changes in experimental conditions.

Table 4-2: Results for the pH investigation

Batch	1	2
pH	5	4
DO	60%	60%
Glucose consumed (g)	17.17	16.97
O_2 consumed (g)	3.77	3.46
Fumaric acid produced (g)	8.45	7.66
Ethanol produced (g)	2.78	2.98
CO_2 produced (g)	4.68	4.80
Succinic acid produced (g)	0.33	0.30
Malic acid produced (g)	0.42	0.47
Glycerol produced (g)	0.91	1.19
Overall fumaric acid yield (g/g)	0.49	0.45
Overall CO_2 yield (g/g)	0.27	0.28
Overall ethanol yield (g/g)	0.16	0.18
Biomass (g)	1.88	1.76
Average fumaric acid production rate (g/g Biomass.h)	0.049	0.043
Average glucose consumption rate (g/g Biomass.h)	0.10	0.10

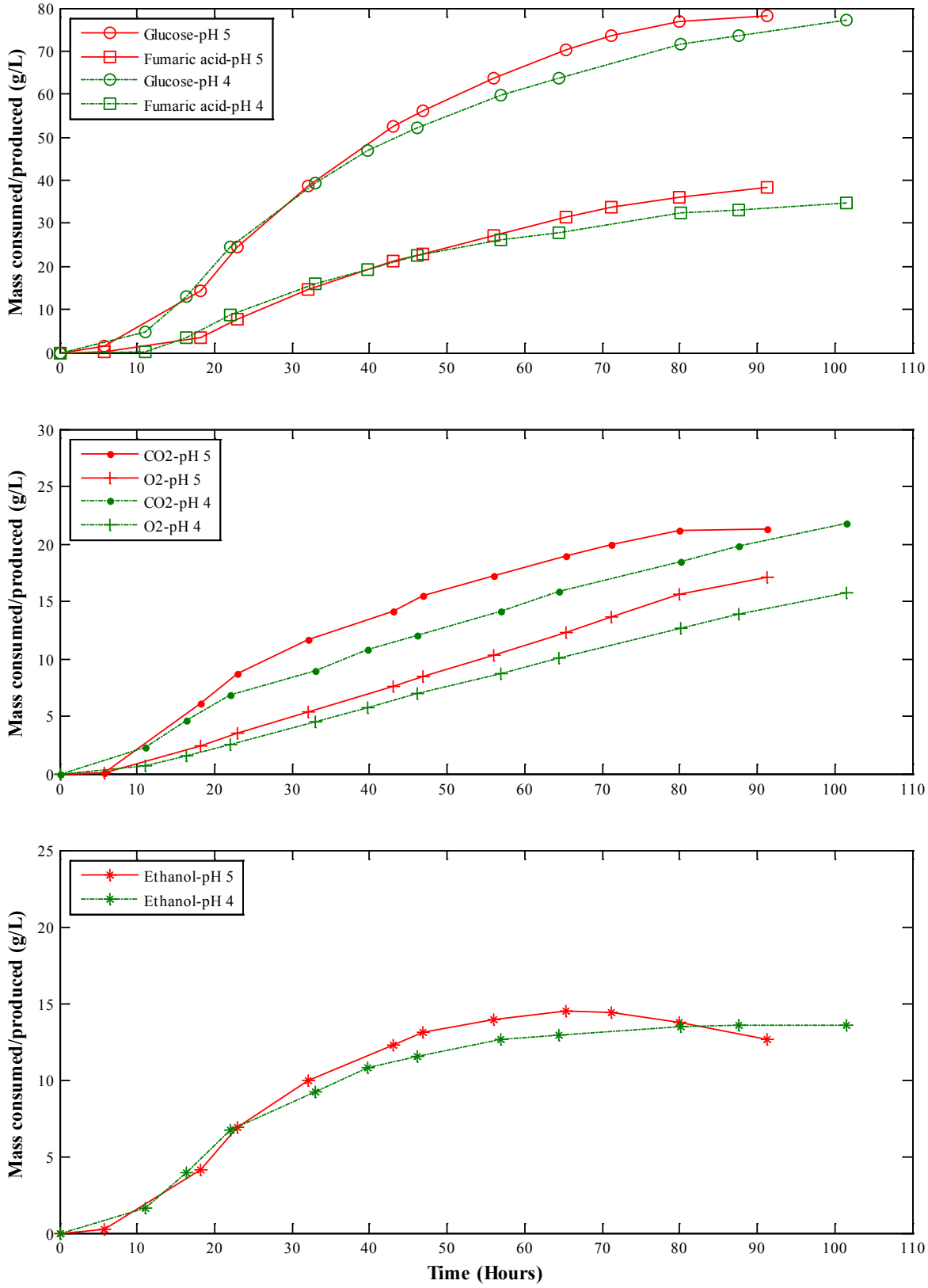

Figure 4-4: Profiles of the pH investigation
The comparisons are between batches 1 and 2. The profiles show reconciled data.

4.3.2 DO results

The profiles for the oxygen requirement investigation are shown in Figure 4-5. The oxygen requirement investigation compares batches 1, 3 and 4. Just as with the pH investigation, only the main product profiles are shown in Figure 4-5, while the minor product profiles are given in Appendix A. The stationary phase for batch 3 was significantly longer than for any of the other batches. This was attributed to the process conditions and, accordingly, no time shift was performed as in Figure 4-3. A summary of the results for the oxygen requirement investigation is given in Table 4-3. The results show a slight difference in biomass.

Table 4-3: Results for the oxygen requirement investigation

Batch	1	3	4
pH	5	5	5
DO	60%	80%	20%
Glucose consumed (g)	17.17	17.07	18.61
O_2 consumed (g)	3.77	2.89	1.30
Fumaric acid produced (g)	8.45	8.83	6.76
Ethanol produced (g)	2.78	2.82	5.54
CO_2 produced (g)	4.68	3.38	4.55
Succinic acid produced (g)	0.33	0.33	0.28
Malic acid produced (g)	0.42	0.56	0.36
Glycerol produced (g)	0.91	1.14	0.69
Overall fumaric acid yield (g/g)	0.49	0.52	0.36
Overall CO_2 yield (g/g)	0.27	0.20	0.24
Overall ethanol yield (g/g)	0.16	0.17	0.30
Biomass (g)	1.88	1.63	1.49
Average fumaric acid production rate (g/g Biomass.h)	0.049	0.044	0.039
Average glucose consumption rate (g/g Biomass.h)	0.10	0.08	0.11

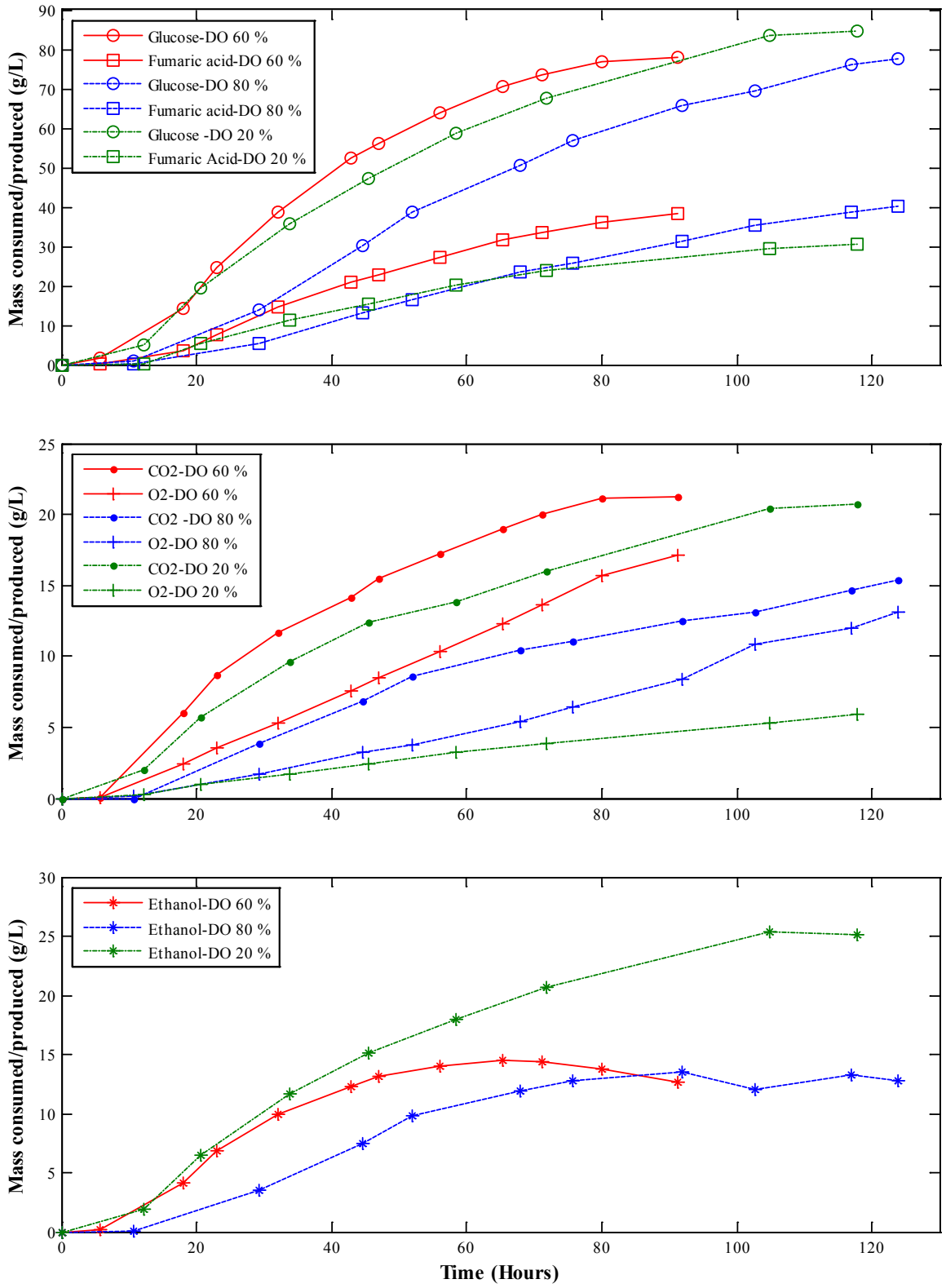

Figure 4-5: Profiles of the oxygen requirement investigation
The comparisons are between batches 1, 3 and 4. The profiles show reconciled data.

5 Discussion

5.1 Time-dependent flux observations

It is evident from the investigation that there are three distinct phases in the fermentation profiles (Figure 4-4 and Figure 4-5) of the production stage. Each phase had a distinctive flux distribution and should be analysed to determine where the rate of production and the yield of fumaric acid is favourable. This will guide the design of future fermentation experiments with the intention of prolonged or continuous operation within these phases. Phase A is identified by the initial period of zero fumaric acid production, Phase B starts with the commencement of fumaric acid production, and phase C starts when ethanol production reaches zero. Figure 5-1 demonstrates how these phases were determined from the fermentation profiles.

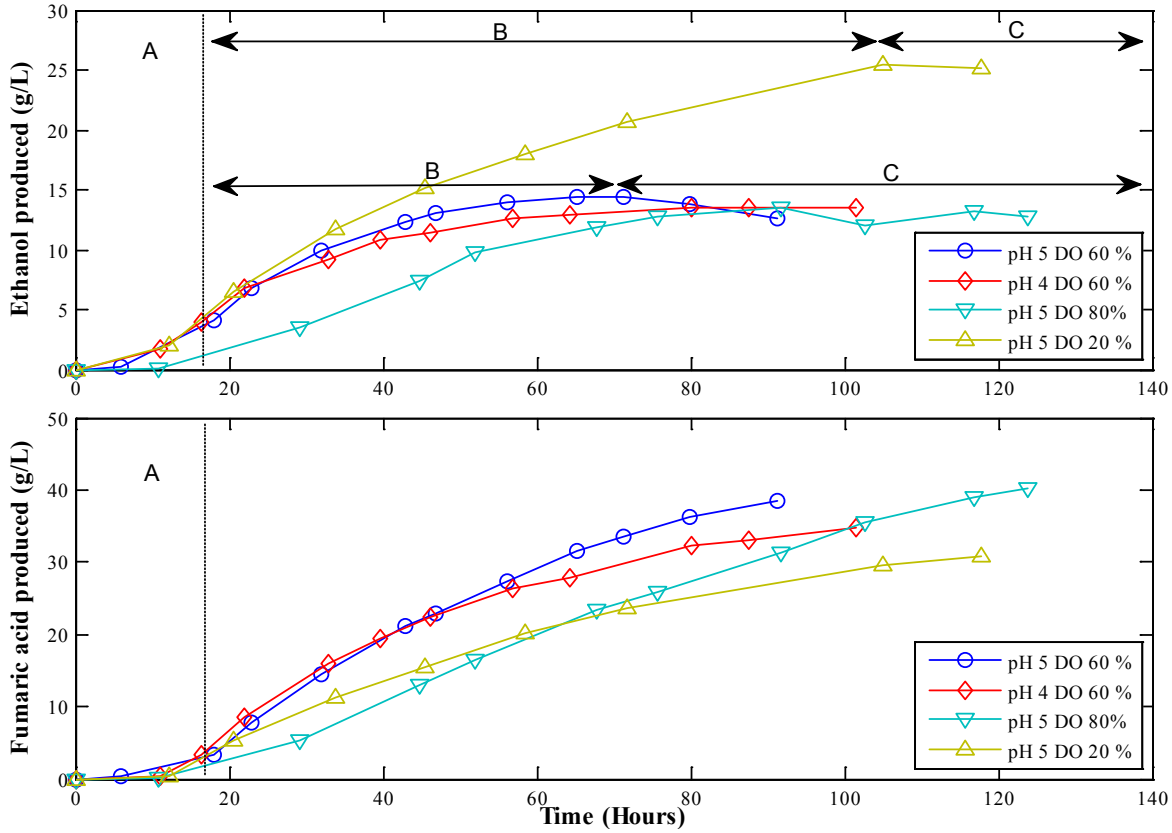

Figure 5-1: Identifying the three different metabolic phases
The ethanol and fumaric acid profiles from Figure 4-4 and Figure 4-5 are shown. Phase A is identified from the fumaric acid profiles, while Phases B and C are identified from the ethanol profiles. The Phase B/C boundary for the DO 20% fermentation varied significantly from that of the other fermentations.

Phase A relates to the acclimatisation period experienced by the biomass when transferred between the growth medium and the fermentation medium, and it results in low glucose consumption rates (Figure 4-4 and Figure 4-5). The fact that there was zero fumaric acid production during this phase implies that all of the glucose was used to generate the energy required for acclimatisation and that the energy was developed from the ethanol and respiration pathways (Section 2.2.2). The oxygen profiles in Figure 4-4 and Figure 4-5 indicate that the glucose flux directed towards the ethanol pathway was the most active during this phase since respiration only commences at the end of the phase, and therefore the bulk of the energy is generated by the ethanol pathway during Phase A. Phase A had an average energy requirement of 0.48 mmol ATP/g Biomass.h, with a standard deviation (σ) of 0.12 mmol ATP/g Biomass.h. The average length of Phase A was 18 hours, which corresponds to between 12% and 18% of the total batch fermentation time. Shortening the length of Phase A could lead to significant increases in overall fumaric acid productivity.

The accumulative nature of the batch profiles in Figure 4-4 and Figure 4-5 makes it difficult to observe the instantaneous flux and rate characteristics for Phases B and C. These characteristics are related to the slopes of these fermentation profiles and a smooth slope was acquired by fitting a third-order polynomial to the profiles in Figure 4-4 and Figure 4-5. These slopes were only fitted between data points where meaningful glucose consumption rates were observed to ensure an accurate representation of the instantaneous metabolic flux. For this reason, the first 20 hours (Phase A) as well as the final 10–15 hours of the batch profiles (Figure 4-4 and Figure 4-5) were not analysed using instantaneous flux characteristics. The fitted polynomials therefore describe only Phase B and most of Phase C. These fitted polynomials are shown in Appendix B and the results of these fitted rates will be presented as instantaneous rates or yields.

5.2 Influence of pH on the metabolic flux distribution

The instantaneous rate of glucose consumption for batches 1 and 2 is given in Figure 5-2. The metabolic flux model was used to divide the glucose consumption rate into separate rates towards the three dominant pathways. These rates are: glucose used for respiration ($r_G{}^R$); glucose used in the ethanol pathway ($r_G{}^E$); and glucose used for fumaric acid production ($r_G{}^F$). They are stacked on top of one another in Figure 5-2. Given the small amount of by-

products, these stacked rates (Figure 5-2) are representative of the total glucose consumption rate ($r_G{}^T$). Instantaneous yields can be obtained intuitively by comparing the thickness of each of the coloured areas.

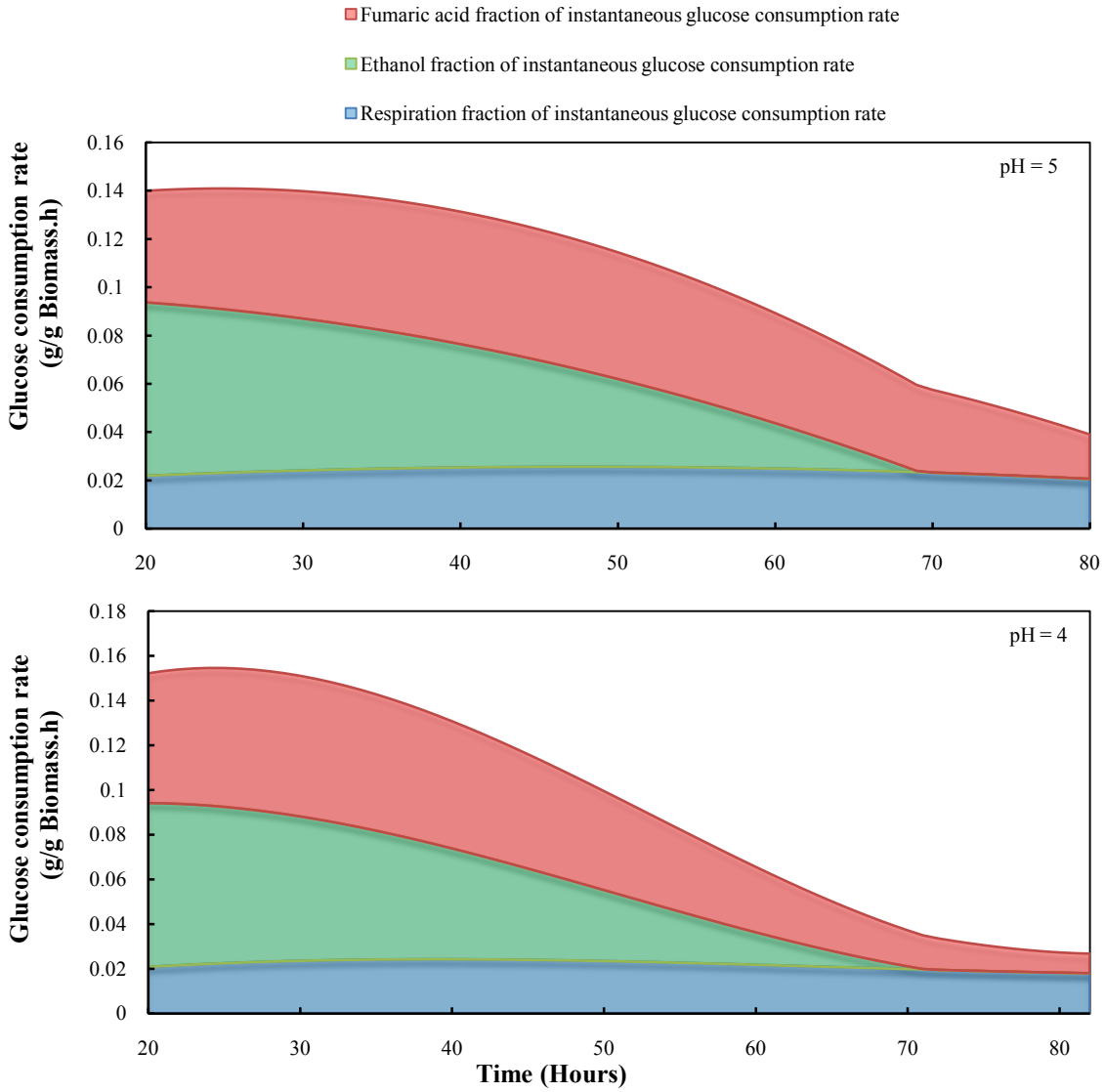

Figure 5-2: Glucose consumption rate for batches 1 and 2
The top graph represents batch 1 (pH 5) and the bottom graph represents batch 2 (pH 4). The area plot represents the stacked rate of glucose consumption towards the three main pathways ($r_G{}^E$, $r_G{}^R$ and $r_G{}^F$); the total area represents more than 90% of the total glucose consumption rate ($r_G{}^T$).

The instantaneous ATP generation rates from the ethanol and respiration pathways are given in Figure 5-3. Similar to the glucose consumption rate in Figure 5-2, the total ATP production rate in Figure 5-3 was split into the two ATP production pathways using the metabolic flux model. The rates are ATP produced from respiration ($r_{ATP}{}^R$) and ATP produced from the ethanol pathway ($r_{ATP}{}^E$). These rates are stacked in Figure 5-3 and the top line represents the

total amount of ATP used for maintenance purposes ($r_{ATP}{}^{T}$). The instantaneous ATP yields can again be obtained intuitively by comparing the thickness of the different coloured areas.

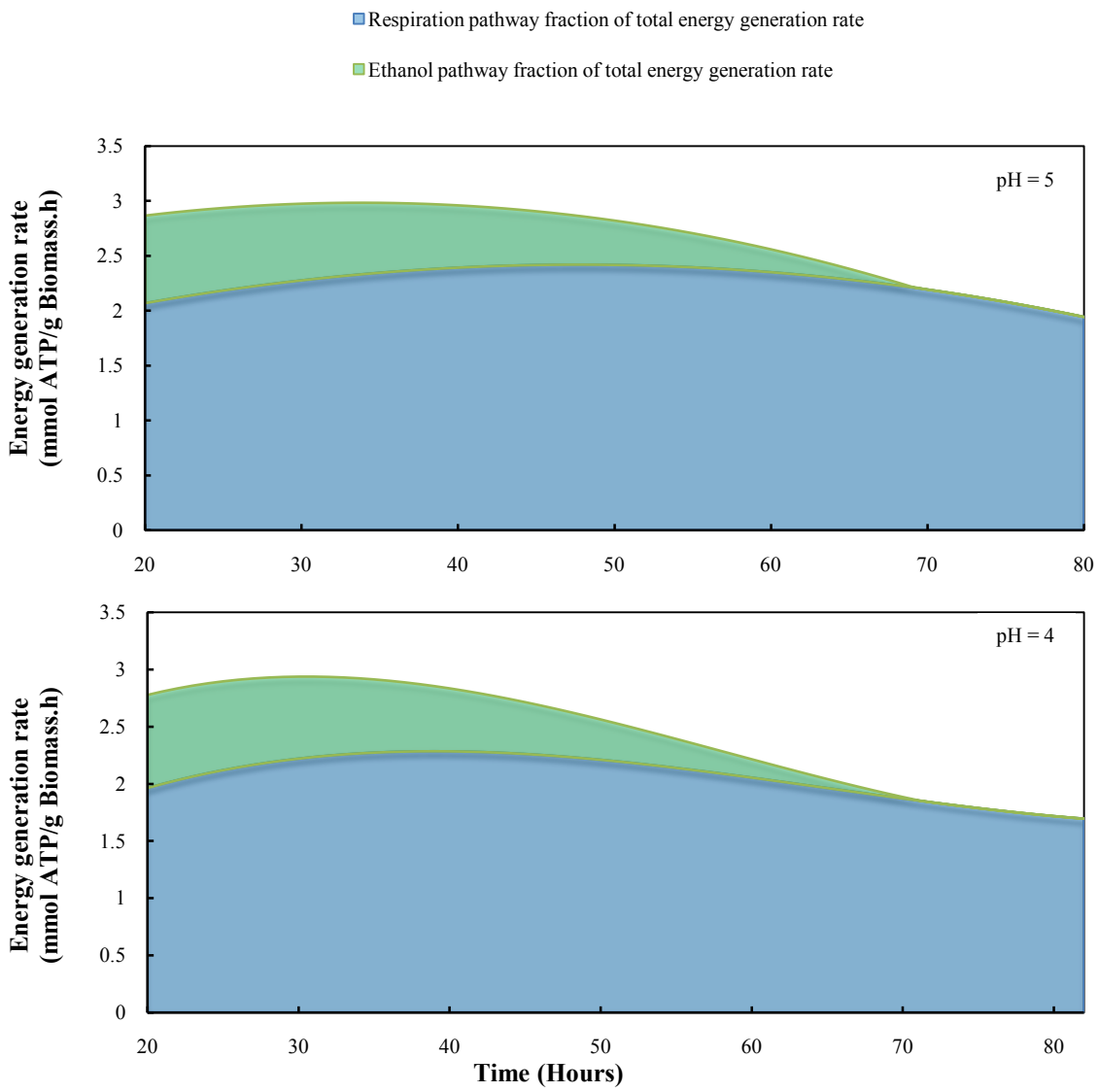

Figure 5-3: ATP production rate for batches 1 and 2
The top graph represents batch 1 (pH 5) and the bottom graph represents batch 2 (pH 4). The area plot represents the stacked rate of ATP production from the ethanol ($r_{ATP}{}^{E}$) and respiration ($r_{ATP}{}^{R}$) pathways. The top line represents the total ATP production rate ($r_{ATP}{}^{T}$) for maintenance purposes (maintenance coefficient). Separate ATP production rates are given by the line profiles.

The first prominent observation from Figure 5-2 is the considerable decrease in $r_G{}^{T}$ for batches 1 and 2 as time proceeds. It can further be seen that $r_G{}^{E}$ declines up to a point where zero ethanol is formed ($r_G{}^{E} = 0$) – this is where the fermentation proceeds from Phase B to Phase C. In contrast to ethanol production, respiration ($r_G{}^{R}$) occurs at a constant rate over time. This implies that the total energy production rate ($r_{ATP}{}^{T}$) decreases with time as the ethanol component diminishes (Figure 5-3). The biomass in total thus requires less energy

(ATP) as time proceeds. This can be interpreted as inactivation of the biomass, although this inactivation occurs only in the anaerobic (ethanol) part of the biomass. It is unclear whether these parts are spatially separated.

The value of r_G^F is crucial for this study and from Figure 5-2 it is clear that r_G^F decreases with time even after r_G^E has reached zero (Phase C). It is postulated that fumarate production is inhibited by the fumaric acid concentration in the broth; this inhibition effect becomes more significant during Phase C of the fermentation (Figure 5-2) due to high fumarate concentrations (> 25 g/L) (Figure 4-4). The distinct difference in the magnitude of r_G^F between the pH 5 (batch 1) and pH 4 (batch 2) fermentations during Phase C is worth noting. The larger r_G^F for the pH 5 fermentation suggests that fumarate inhibition is less severe at a high pH.

The relation between r_G^F and r_G^T (fumaric acid yield) during the fermentation is another crucial parameter in this study. The bulk of the fumaric acid for all the batches was produced during Phase B (Figure 4-4 and Figure 4-5). Ethanol production during Phase B is a major waste of substrate (Figure 5-2), since its contribution to energy generation is minimal (Figure 5-3). r_G^E and r_{ATP}^E are at a maximum at the start of Phase B and diminish with time until ethanol production ceases. The consequence of this is that the instantaneous fumaric acid yield (Y_{GF}^{inst}) increases with time during Phase B until it reaches its maximum at the end of Phase B, as shown in Figure 5-4. However, as a result of the high r_G^E at the start of Phase B, the impact of the improved Y_{GF}^{inst} on the accumulative yield is minimal (Figure 5-4).

It is evident that Y_{GF}^{inst} is decreasing with time during Phase C (Figure 5-4) due to fumarate inhibition. The effect is less severe for the higher pH fermentation (pH 5), as demonstrated by the higher Y_{GF}^{inst}. However, this was not observed from the accumulative yields (Table 4-2 and Figure 5-4) due to the small amount of fumaric acid produced in Phase C. Nevertheless, the accumulative outcome of the fermentation is likely to be affected if most of the fumaric acid is produced during this phase. This can be achieved by utilising higher initial glucose concentrations, which ties in with the results shown in Table 2-1, where the fermentations with the highest fumaric acid titres (high initial glucose concentrations) also had the highest fumaric acid yields. Alternatively, continuous operation can also be considered to utilise the observed high instantaneous yields. Such a set-up would have to be operated at the start of

Phase C as it will result in favourable fumaric acid yields (Figure 5-4) and production rates (Figure 5-2).

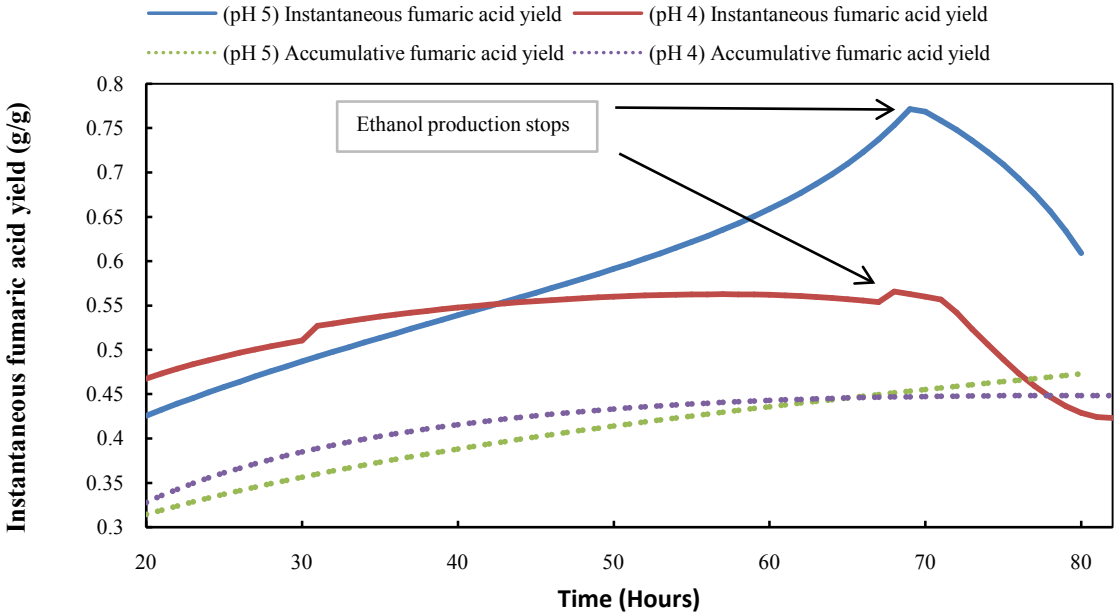

Figure 5-4: Instantaneous and accumulative fumaric acid yields for batches 1 and 2

5.3 Influence of DO on the metabolic flux distribution

Graphs similar to those used in the pH discussion (Figure 5-2, Figure 5-3 and Figure 5-4) were generated for the DO comparison. The first distinct difference from Figure 5-5 lies in the value of $r_G{}^R$ for the different DO levels. The oxygen consumption rate for the DO 20% fermentation was noticeably lower than for the other two fermentations (Figure 4-5) and is reflected by a constant $r_G{}^R$ rate (0.01g/g Biomass.h) that is half of that for the DO 60% fermentation (0.02 g/g Biomass.h). By comparison, the DO 80% fermentation attained an identical $r_G{}^R$ rate to the DO 60% fermentation, but only once Phase C had commenced. The $r_G{}^R$ rate for the DO 80% fermentation increased gradually during Phase B until it reached 0.02 g/g Biomass.h. It is therefore apparent that there is a maximum respiration capacity (0.8 mmol O_2/g Biomass.h), which corresponds to an $r_G{}^R$ of 0.02 g/g Biomass.h. The DO 60% fermentation functions at maximum respiration capacity during Phases B and C, while the DO 80% fermentation functions at full capacity only during Phase C. In contrast, the DO 20% fermentation functions at only half of its full respiration capacity. The maximum respiration capacity is presumably linked to the identical growth method employed for all three fermentations.

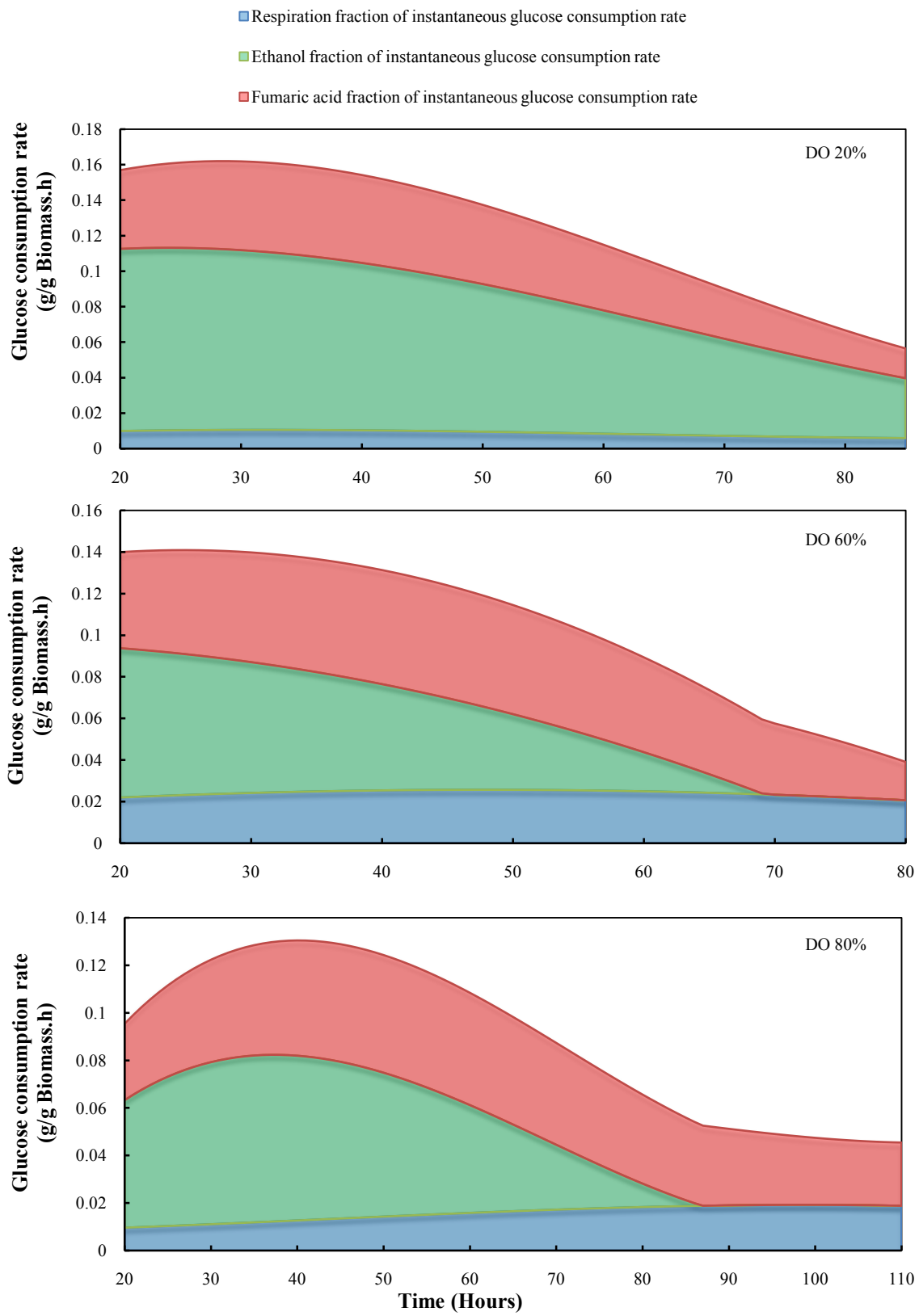

Figure 5-5: Glucose consumption rate for batches 1, 3 and 4
The top graph represents batch 4 (DO 20%), the middle graph represents batch 1 (DO 60%) and the bottom graph represents batch 3 (DO 80%). The area plot represents the stacked rate of glucose consumption towards the three main pathways (r_G^E, r_G^R and r_G^F), and the total area represents more than 90% of the total glucose consumption rate (r_G^T).

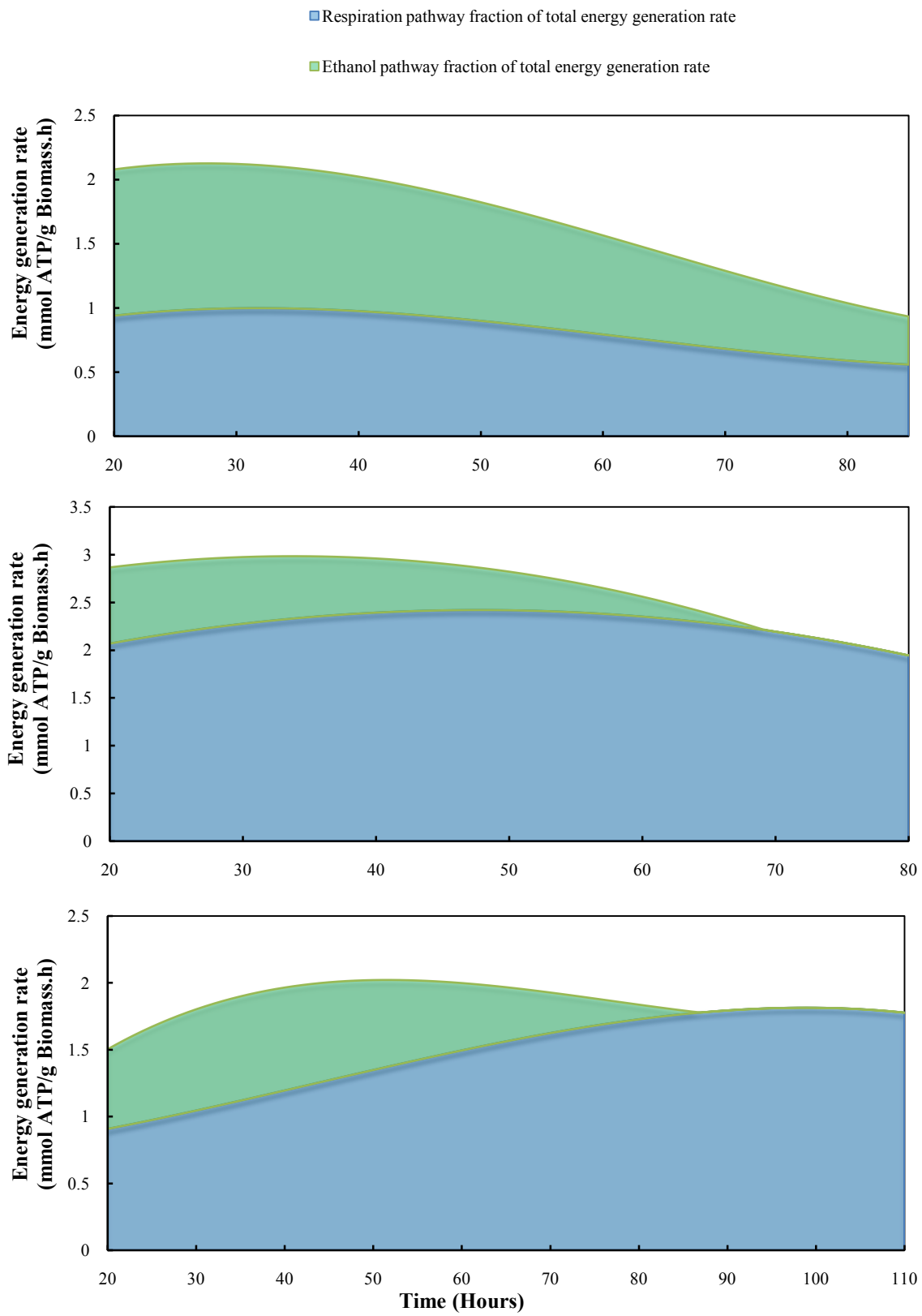

Figure 5-6: ATP production rate for batches 1, 3 and 4
The top graph represents batch 4 (DO 20%), the middle graph represents batch 1 (DO 60%) and the bottom graph represents batch 3 (DO 80%). The area plot represents the stacked rate of ATP production from the ethanol (r_{ATP}^{E}) and respiration (r_{ATP}^{R}) pathways. The top line represents the total ATP production rate (r_{ATP}^{T}) for maintenance purposes (maintenance coefficient).

Ethanol production (r_G^E) in Figure 5-5 was noticeably different for all three fermentations. The DO 20% fermentation always had the highest r_G^E. r_G^E reached zero at 105 hours (Figure 4-5), which was much later than for the other fermentations and falls outside the time scale for Figure 5-5 and Figure 5-6. A substantial fraction of the ATP was generated from the ethanol pathway (r_{ATP}^E), as revealed in Figure 5-6. The total ATP production rate (r_{ATP}^T = 2 mmol ATP/g Biomass.h) was similar to that of maximum respiration capacity for the other two fermentations (r_{ATP}^R = 2 mmol ATP/g Biomass.h) but diminished with time. With the DO 80% fermentation the initial r_G^E was higher than that of the DO 60% fermentation, which was probably a response to the lowered r_G^R at the start of Phase B.

Fumaric acid production rate (r_G^F) for the DO 20% fermentation was lower than that of the other fermentations and declined as time proceeded. Similar r_G^F rates were observed for the DO 60% and 80% fermentations, although the r_G^F for the DO 60% fermentation decreased more severely during Phase C. This suggests that the fumarate inhibition at high fumaric acid concentrations is less profound at higher DO levels, despite the fact that the oxygen consumption rates were similar during Phase C.

The instantaneous and accumulative yields are plotted as a function of time in Figure 5-7. Similar to what was found in the pH investigation (Figure 5-4), the instantaneous fumaric acid yield (Y_{GF}^{inst}) increases with time during Phase B until the maximum is reached at the end of Phase B for the DO 60% and 80% fermentations. However, as a result of the high r_G^E during Phase B, the impact of the increased Y_{GF}^{inst} on the accumulative yield is less pronounced. As with the pH investigation, Y_{GF}^{inst} decreases during Phase C due to fumarate inhibition. This effect is, however, less severe for the DO 80% fermentation which relates to a maintained Y_{GF}^{inst} of 0.8 g/g, whereas the Y_{GF}^{inst} for the DO 60% fermentation decreases substantially. Again, these results are not reflected in the accumulative yields since the amount of fumaric acid produced during Phase C is minimal. Inhibition is, however, expected to influence the accumulative outcome of the fermentation if most of the fumaric acid is produced during this phase. This can be achieved with higher initial glucose concentrations or continuous operation, as discussed earlier.

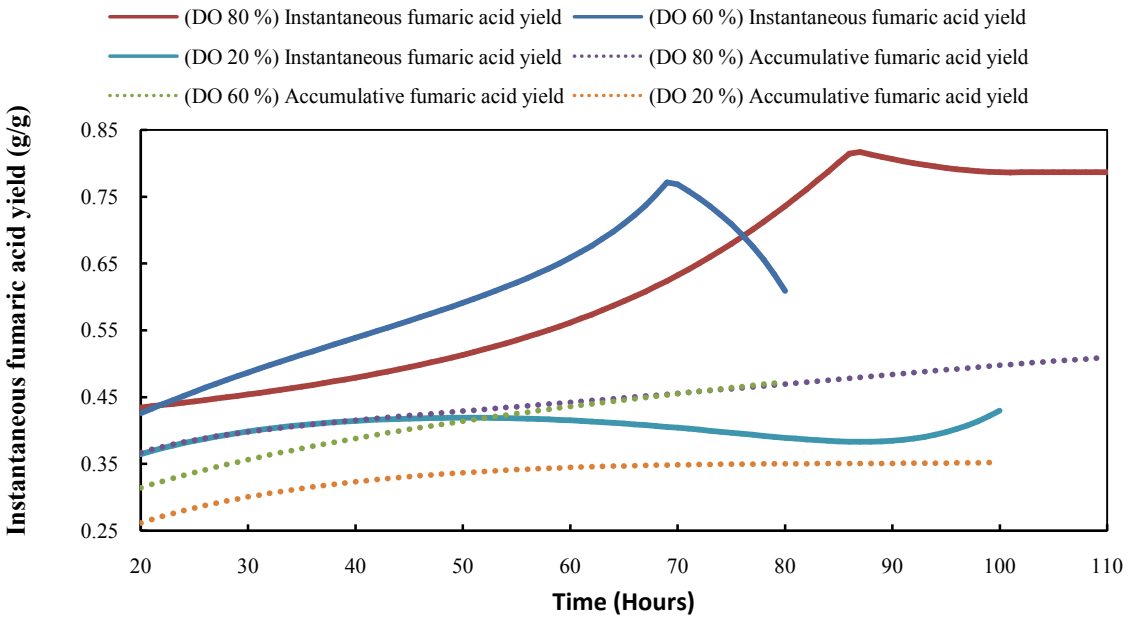

Figure 5-7: Instantaneous and accumulative yields for batches 1, 3 and 4

6 Conclusions and recommendations

In this study the instantaneous metabolic flux distribution of *Rhizopus oryzae* (ATCC 20344) was investigated by means of mass-based data reconciliation, which resulted in improved measurement accuracy. This led to the identification of various metabolic flux phases which can be exploited in order to increase fumaric acid yield and productivity. Three distinct metabolic phases were present during the production stage of fumaric acid fermentation. Phase A was characterised by zero fumaric acid production, which relates to the adaptation period when changing from the growth to the fermentation medium. During Phase A most of the required energy was produced from the ethanol pathway. During Phase B glucose was directed towards all three of the major pathways (fumaric acid [$r_G{}^F$], ethanol [$r_G{}^E$] and respiration [$r_G{}^R$]). Most of the glucose was consumed through the ethanol pathway, while most of the energy (ATP) was produced from the respiration pathway. Ethanol production declined during Phase B until $r_G{}^E = 0$, which marked the start of Phase C in which glucose was directed only towards the fumaric acid and respiration pathways.

The decline in $r_G{}^E$ was interpreted as an inactivation of biomass. However, the respiration capacity ($r_G{}^R$) did not deteriorate with time. This suggests that the inactivation occurs only in the anaerobic 'part' of the biomass, although it is not clear how these 'parts' are separated. The biomass exhibited a constant and identical $r_G{}^R$ of 0.02 g glucose/g Biomass.h (O_2 consumption rate of 0.8 mmol O_2/g Biomass.h) for all the DO 60% and 80% fermentations, which implies that $r_G{}^R$ is bounded to a maximum value which could be related to the growth method. With limited oxygen supply (DO 20%) the full respiration capacity was not achieved, whereas under high oxygen concentrations (DO 80%) full respiration capacity was achieved only after the DO 60% fermentations.

Ethanol production during Phase B accounted for a major fraction of the glucose consumed; therefore the overall fumaric acid yields (0.52 g/g for DO 80%) were much lower than the high instantaneous yields (up to 0.8 g/g for DO 80%) obtained during Phase C. The fact that the respiration rate remains constant throughout Phase C implies that the instantaneous fumaric acid yield is dictated solely by the fumaric acid production rate during this phase. It was found that this rate is inhibited by the fumarate concentration itself, which is why maximum instantaneous fumaric acid yields were always obtained at the start of Phase C.

This inhibition effect was more severe at a pH of 4, whereas higher DO levels (80%) reduced this effect.

The design of future batch fermentations, based on the results of this study, should ensure that most of the fumaric acid is produced during Phase C. This can be achieved by using higher initial glucose fermentations. Continuous operation at initial Phase C conditions is another attractive option. This should enable high accumulative fumaric acid yields (up to 0.8 g/g) to be achieved and should be the target for future fumaric acid studies.

7 References

Abe, A. et al., 2003. rDNA ITS sequence of *Rhizopus oryzae*: its application to classification and identification of lactic acid producers. *Bioscience, Biotechnology and Biochemistry*, 67(8): 1725–1731.

Cao, N. et al., 1996. Simultaneous production and recovery of fumaric acid from immobilized rhizopus oryzae with a rotary biofilm contactor and an adsorption column. *Applied and Environmental Microbiology*. 62(8): 2926-2931.

Cao, N. et al., 1997. Production of fumaric acid by immobilized rhizopus using rotary biofilm contactor. *Applied Biochemistry and Biotechnology*, 63–65: 387–394.

Carta, F.S. et al., 1999. Production of fumaric acid by fermentation of enzymatic hydrolysates derived from cassava bagasse. *Bioresource Technology*, 68(1): 23–28.

Deng, Y. et al., 2012. Production of fumaric acid by simultaneous saccharification and fermentation of starchy materials with 2-deoxyglucose-resistant mutant strains of Rhizopus oryzae. *Bioresource Technology*, 107: 363–367.

Ding, Y. et al., 2011. Production of fumaric acid by *Rhizopus oryzae*: role of carbon-nitrogen ratio. *Applied Biochemistry and Biotechnology*, 164(8): 1461–1467.

Du, J. et al., 1997. Fumaric acid production in airlift loop reactor with porous sparger. *Applied biochemistry and Biotechnology*, 63-65: 541–556.

Foster, J. & Waksman, S., 1939. The production of fumaric acid by molds belonging to the genus *Rhizopus*. *Journal of the American Chemical Society*, 61: 127-135.

Fu, Y. et al., 2009. A novel multi-stage preculture strategy of *Rhizopus oryzae* ME-F12 for fumaric acid production in a stirred-tank reactor. *World Journal of Microbiology and Biotechnology*, 25(10): 1871–1876.

Fu, Y.-Q. et al., 2010. Enhancement of fumaric acid production by *Rhizopus oryzae* using a two-stage dissolved oxygen control strategy. *Applied Biochemistry and Biotechnology*, 162(4): 1031–1038.

Gangl, I., Weigand, W. & Keller, F., 1990. Economic comparison of calcium fumarate and sodium fumarate production by *Rhizopus arrhizus. Applied Biochemistry and Biotechnology*, 24(1): 663-677.

Gangl, I., Weigand, W. & Keller, F., 1991. Metabolic modeling of fumaric acid production byrhizopus arrhizus. *Applied biochemistry and biotechnology*, 28(1): 471-486.

Ghosh, B. & Ray, R.R., 2011. Current commercial perspective of *Rhizopus oryzae*: a review. *Journal of Applied Sciences*, 14: 2470-2486.

Grand View Research, 2014. *Maleic anhydride market analysis by application (unsaturated polyster resins, bdo, additives, copolymers) and segment forecasts to 2020.*San Francisco, CA, US.

Grimm, L.H. et al., 2005. Morphology and productivity of filamentous fungi. *Applied Microbiology and Biotechnology*, 69(4): 375–384.

Gu, C. et al., 2013. Production of fumaric acid by immobilized *Rhizopus arrhizus* on net. *Bioresource Technology*, 131: 303–307.

Huang, L. et al., 2010. High-throughput screening of high-yield colonies of *Rhizopus oryzae* for enhanced production of fumaric acid. *Annals of Microbiology*, 60(2): 287–292.

IHS, 2014. *Chemical Economics Handbook – Fumaric acid*. Available at: http://ihs.com.

Jang, Y.-S. et al., 2012. Bio-based production of C2-C6 platform chemicals. *Biotechnology and Bioengineering*, 109(10): 2437–2459.

Kang, S.W. et al., 2010. Strain development and medium optimization for fumaric acid production. *Biotechnology and Bioprocess Engineering*, 15(5): 761–769.

Kenealy, W. et al., 1986. Biochemical aspects of fumaric acid accumulation by *Rhizopus arrhizus*. *Applied and Environmental Microbiology*, 52(1): 128–133.

Liao, W. et al., 2007. A new approach of pellet formation of a filamentous fungus – *Rhizopus oryzae*. *Bioresource Technology*, 98(18): 3415–3423.

Ling, L.B. & Ng, T.K., 1989. Fermentation process for carboxylic acids. US Patent 4,877,731.

Liu, Y., Liao, W. & Chen, S., 2008. Study of pellet formation of filamentous fungi *Rhizopus oryzae* using a multiple logistic regression model. *Biotechnology and Bioengineering*, 99(1): 117–128.

Lohbeck, K. et al., 1990. Maleic and fumaric acids. In *Ullmann's Encyclopedia of Industrial Chemistry*, Vol. A16, Wiley, Winheim, Germany.

Markets and Markets, 2014. *Feed Acidifiers Market By Type, Livestock & Geography - Global Trends and Forecasts to 2018*. Available at: http://marketsandmarkets.com,

McGinn, S.M. et al., 2004. Methane emissions from beef cattle : Effects of monensin, sunflower oil, enzymes, yeast, and fumaric acid. Journal of Animal Science, 82(11): 3346-3356.

Mondala, A.H., 2015. Direct fungal fermentation of lignocellulosic biomass into itaconic, fumaric, and malic acids: current and future prospects. *Journal of Industrial Microbiology & Biotechnology*, 42(4): 487–506.

Morrin, M. & Ward, O.P., 1990. Relationships between fungal growth, morphology and fumaric acid production by *Rhizopus arrhizus*. *Mycological Research*, 94(4): 505–510.

Ng, T.K. et al., 1986. Production of tetrahydrofuran/1,4 butanediol by a combined biological and chemical process. *Biotechnology and Bioengineerng Symposium,* 17: 344–363.

Osmani, S. A. & Scrutton, M.C., 1985. The sub-cellular localisation and regulatory properties of pyruvate carboxylase from *Rhizopus arrhizus*. *European Journal of Biochemistry / FEBS*, 147(1): 119–128.

Petruccioli, M., Angiani, E. & Federici, F., 1996. Semi-continuous fumaric acid production by *Rhizopus arrhizus* immobilized in polyurethane sponge. *Process Biochemistry*, 31(5): 463–469.

Rhodes, R. A. et al., 1962. Production of fumaric acid in 20-liter fermentors. *Applied Microbiology*, 10(1): 9–15.

Riscaldati, E. et al., 2000. Direct ammonium fumarate production by *Rhizopus arrhizus* under phosphorous limitation. *Biotechnology Letters*: 1043–1047.

Riscaldati, E. & Moresi, M., 2002. Ammonium fumarate production by free or immobilised *Rhizopus arrhizus* in bench-and laboratory-scale bioreactors. *Journal of Chemical Technology*, 77(9): 1013–1024.

Roa Engel, C. A. et al., 2011. Development of a low pH fermentation strategy for fumaric acid production by *Rhizopus oryzae*. *Enzyme and Microbial Technology*, 48(1): 39–47.

Roa Engel, C. A. et al., 2008. Fumaric acid production by fermentation. *Applied Microbiology and Biotechnology*, 78(3): 379–89.

Romano, A.H. et al., 1967. Mechanism of fumaric acid accumulation in *Rhizopus nigricans* *Journal of Bacteriology*, 93: 600–604.

Sauer, M. et al., 2008. Microbial production of organic acids: expanding the markets. *Trends in Biotechnology*, 26(2): 100–108.

Song, P. et al., 2011. Expression and characterization of fumarase (FUMR) from *Rhizopus oryzae*. *Fungal Biology*, 115(1): 49–53.

Villadsen, J., Nielsen, J. & Lidén, G., 2011. *Bioreaction Engineering Principles*. Boston, MA, US: Springer US.

Werpy, T. & Petersen, G., 2004. Top Value Added Chemicals from Biomass: Volume I -- Results of Screening for Potential Candidates from Sugars and Synthesis Gas. US Department of Energy, DOE/GO 102004-1992.

Xu, Q. et al., 2012. Key technologies for the industrial production of fumaric acid by fermentation. *Biotechnology Advances*, 30(6): 1685–1696.

Zhou, Y., Du, J. & Tsao, G.T., 2002. Comparison of fumaric acid production by *Rhizopus oryzae* using different neutralizing agents. *Bioprocess and Biosystems Engineering*, 25(3): 179–81.

Zhou, Y., Du, J. & Tsao, G.T., 2000. Mycelial pellet formation by *Rhizopus oryzae* ATCC 20344. *Applied Biochemistry and Biotechnology*, 84-86: 779–789.

Appendices

Appendix A. Malic acid, glycerol and succinic acid profiles

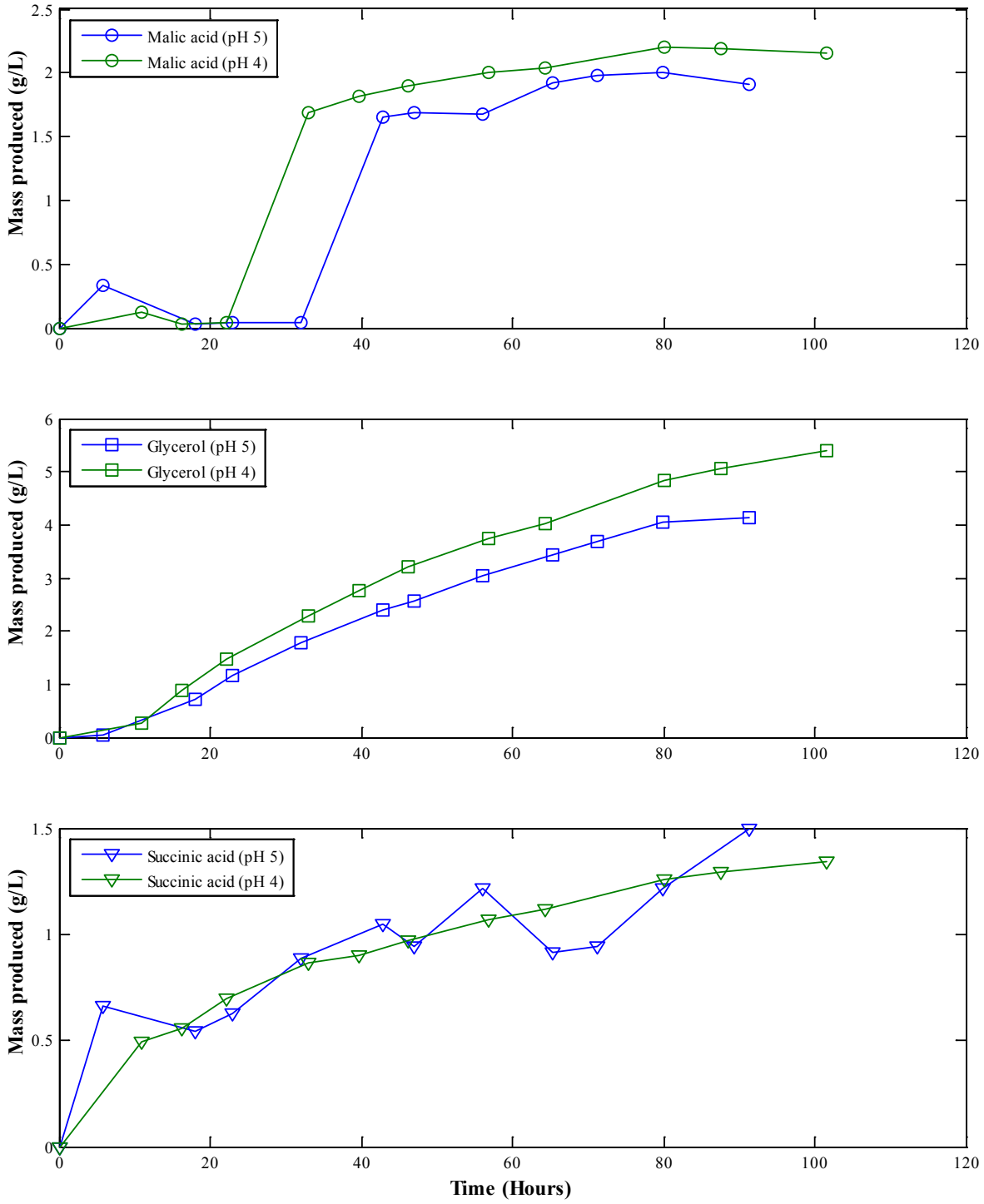

Figure A-1: Malic acid, glycerol and succinic acid profiles for the pH investigation

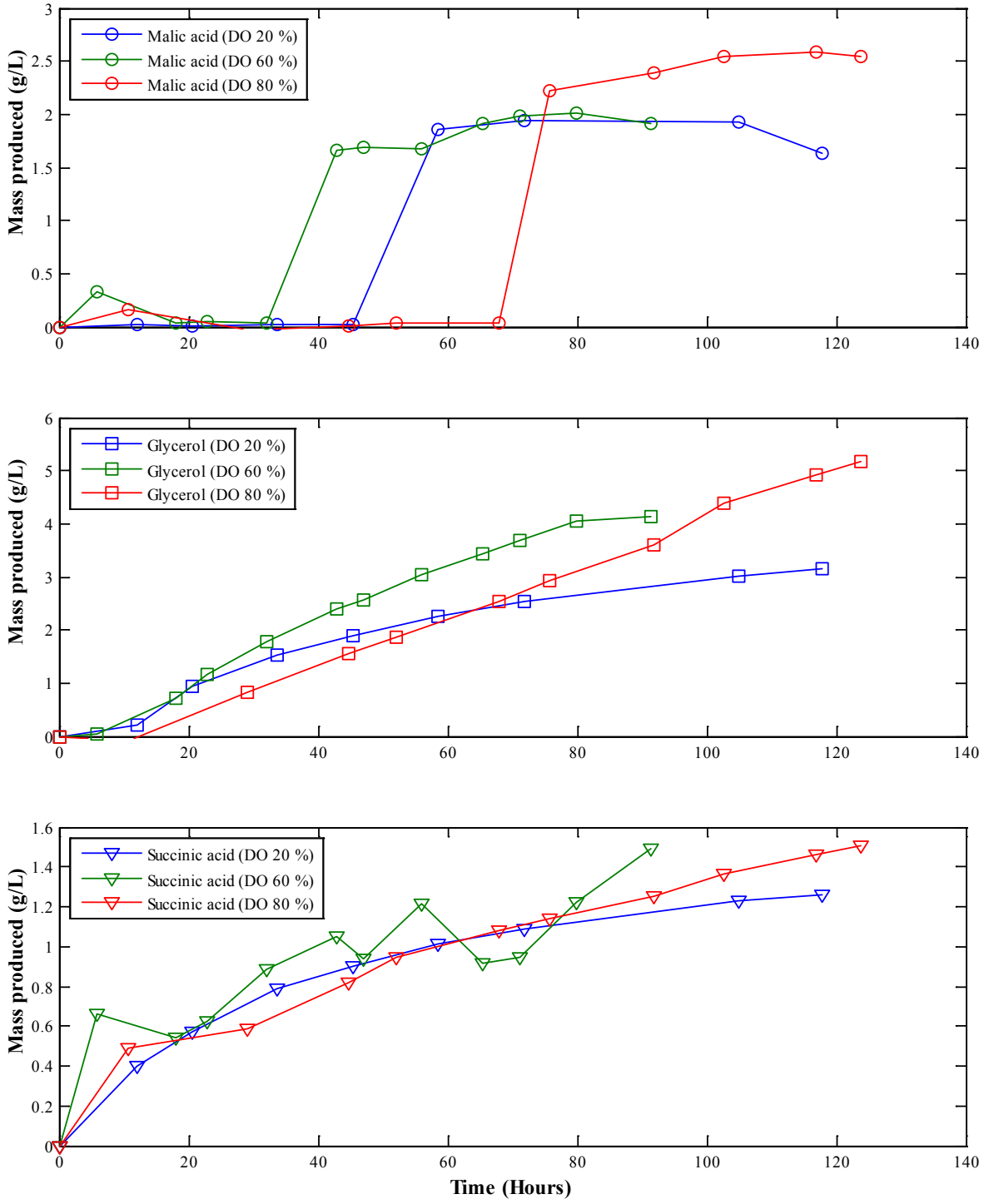

Figure A-2: Malic acid, glycerol and succinic acid profiles for the DO investigation.

Appendix B. Third-order polynomial fit of fermentation data

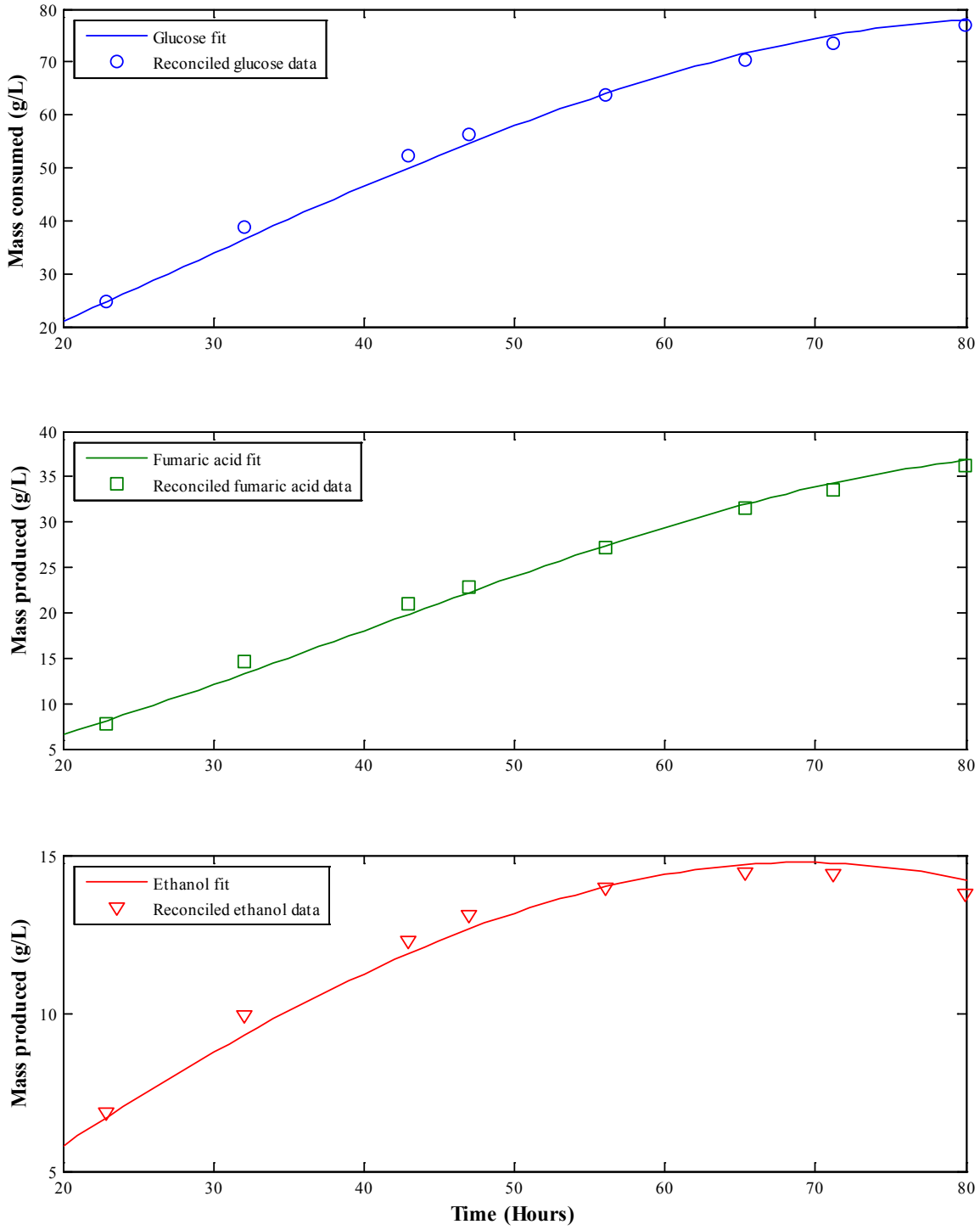

Figure B-1: Third-order polynomial fits for batch No. 1 (pH 5; DO 60%)

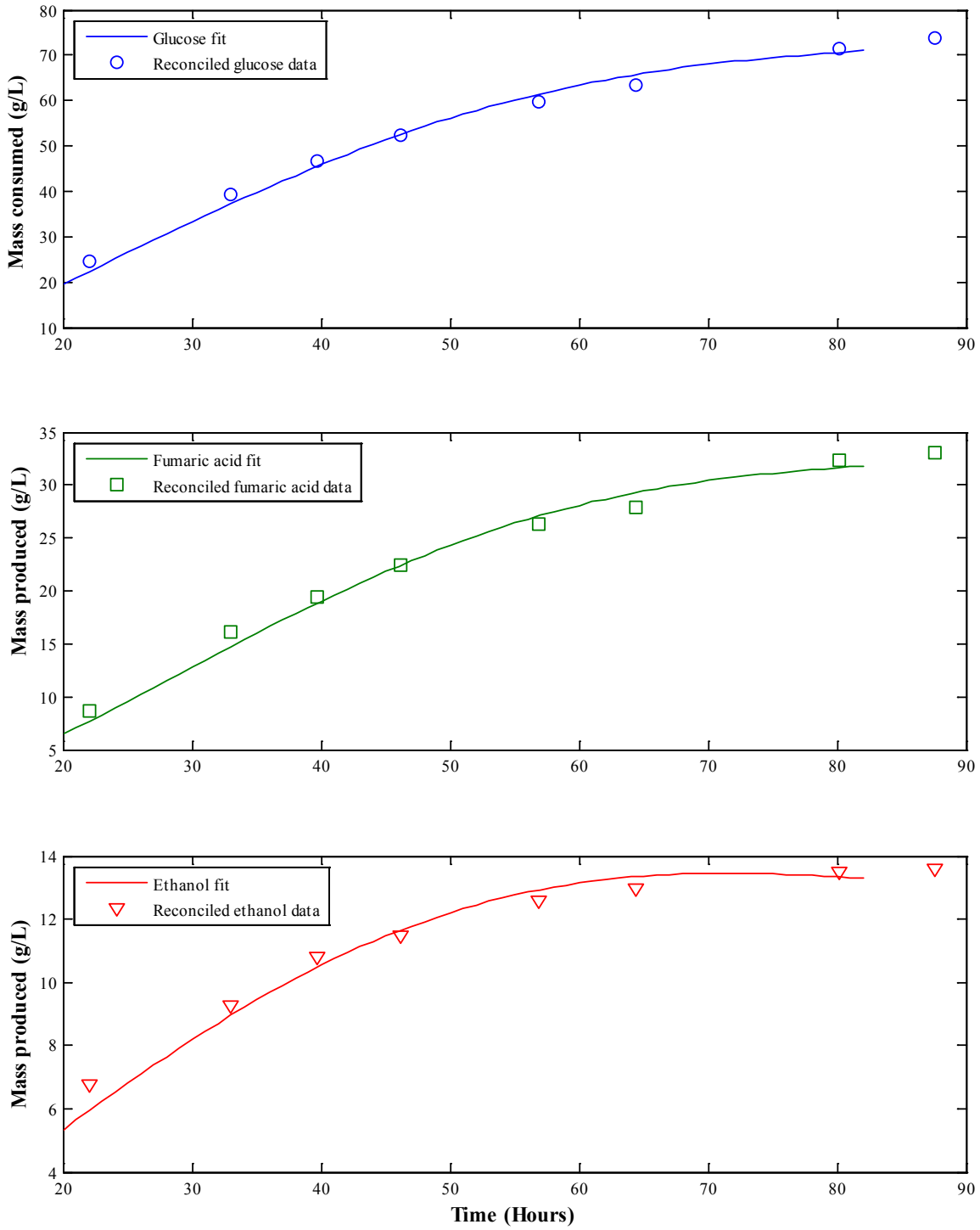

Figure B-2: Third-order polynomial fits for batch No. 2 (pH 4; DO 60%)

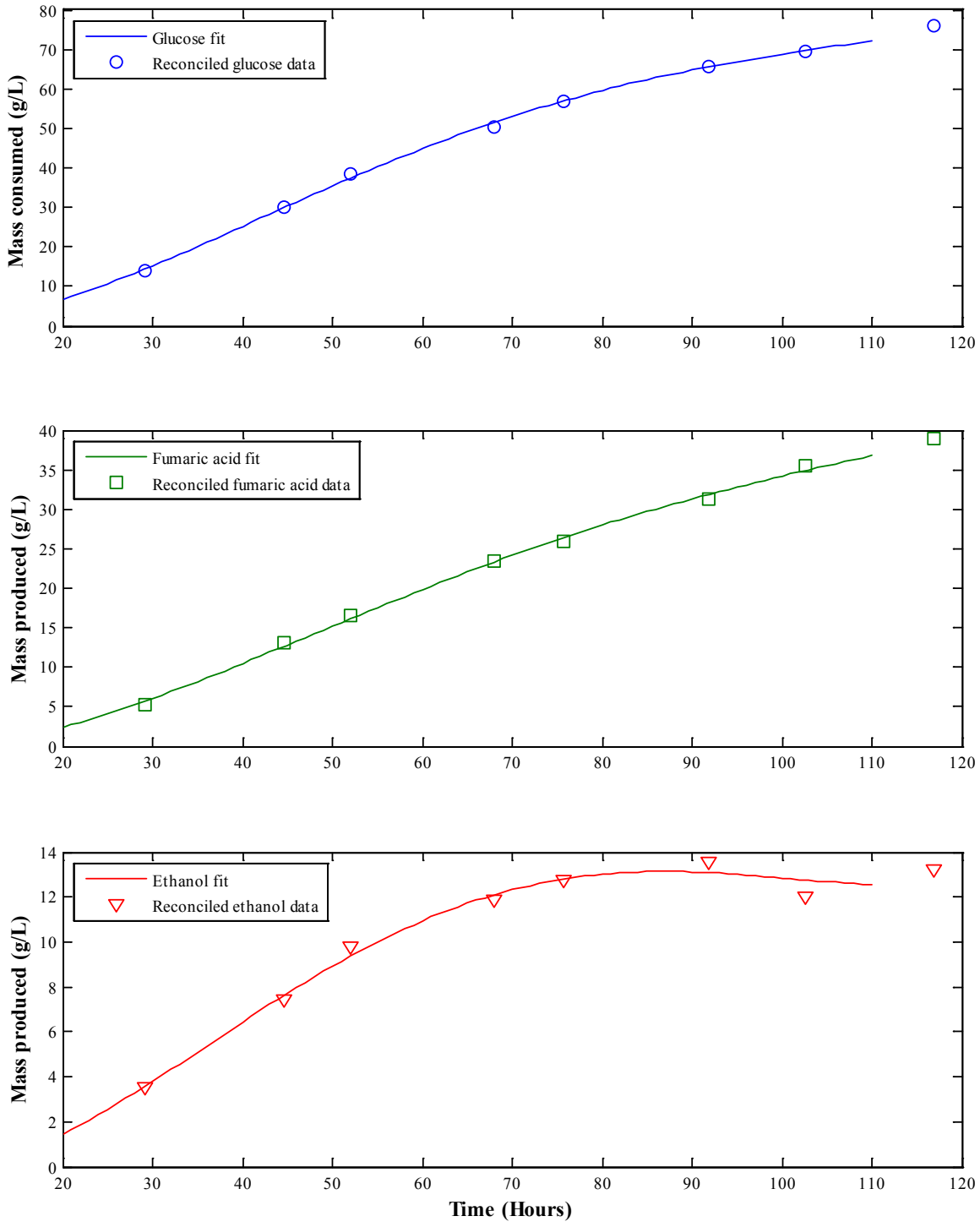

Figure B-3: Third-order polynomial fits for batch No. 3 (pH 5; DO 80%)

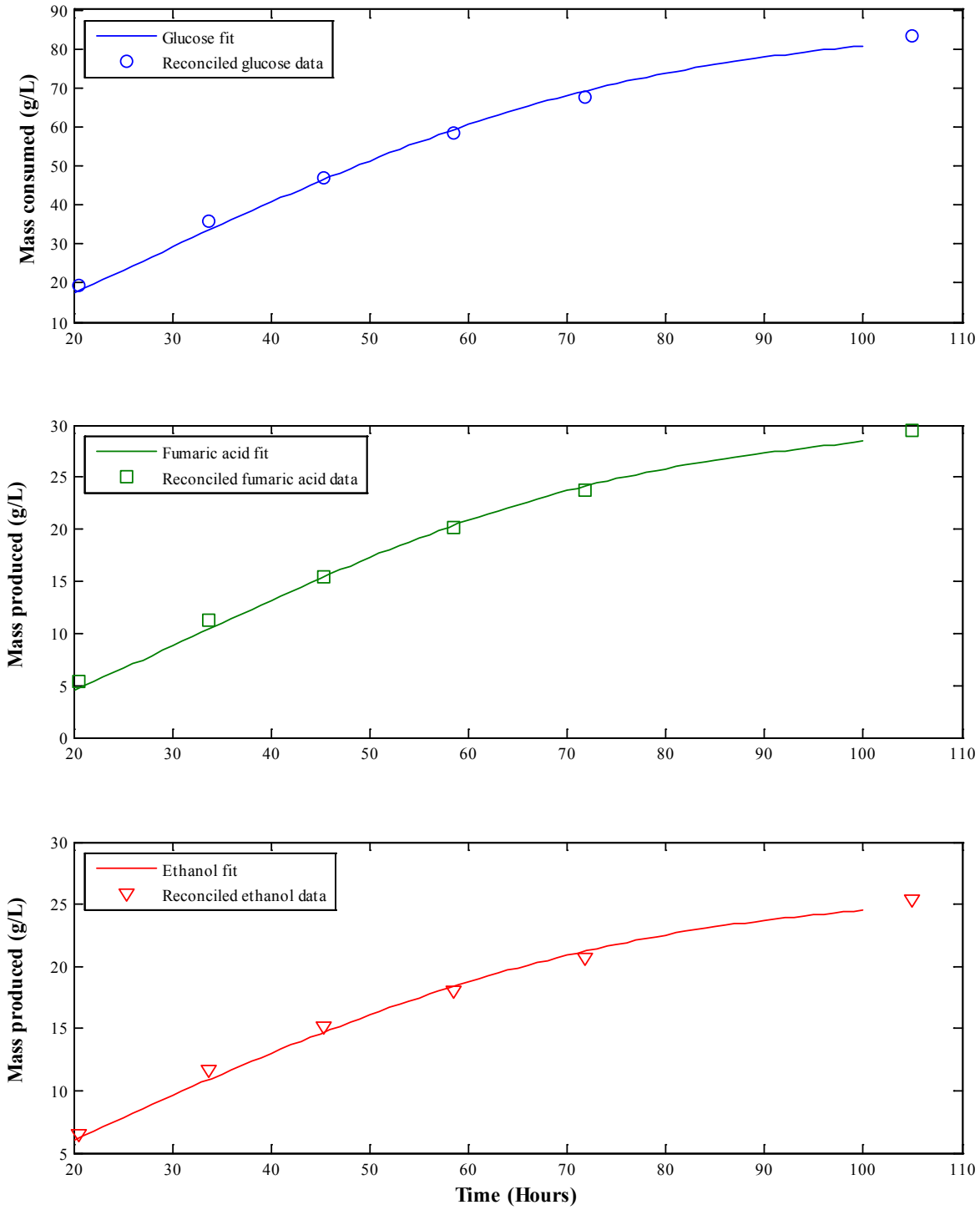

Figure B-4: Third-order polynomial fits for batch No. 4 (pH 5; DO 20%)